Mechanical degradation and stability of organic solar cells: Molecular and microstructural determinants

Journal:	*Energy & Environmental Science*
Manuscript ID:	EE-REV-08-2014-002657.R2
Article Type:	Review Article
Date Submitted by the Author:	17-Oct-2014
Complete List of Authors:	Savagatrup, Suchol; University of California, San Diego, Department of NanoEngineering Printz, Adam; University of California, San Diego, Department of NanoEngineering O'Connor, Timothy; University of California, San Diego, Department of NanoEngineering Zaretski, Aliaksandr; University of California, San Diego, Department of NanoEngineering Rodriquez, Daniel; University of California, San Diego, Department of NanoEngineering Sawyer, Eric; University of California, San Diego, Department of NanoEngineering Rajan, Kirtana; University of California, San Diego, Department of NanoEngineering Acosta, Raziel; University of California, San Diego, Department of NanoEngineering Root, Samuel; University of California, San Diego, Department of NanoEngineering Lipomi, Darren; University of California, San Diego, NanoEngineering

Mechanical degradation and stability of organic solar cells: Molecular and microstructural determinants

Suchol Savagatrup, Adam D. Printz, Timothy F. O'Connor, Aliaksandr V. Zaretski, Daniel Rodriquez, Eric J. Sawyer, Kirtana Rajan, Raziel I. Acosta, Samuel E. Root, and Darren J. Lipomi*

Department of NanoEngineering, University of California, San Diego, 9500 Gilman Drive, Mail Code 0448, La Jolla, CA 92093-0448

*Author to whom correspondence should be addressed: dlipomi@ucsd.edu

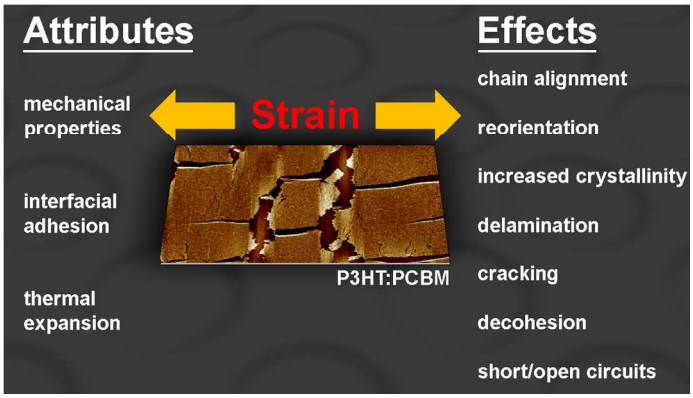

Graphical abstract

Abstract

The mechanical properties of organic semiconductors and the mechanical failure mechanisms of devices play critical roles in the yield of modules in roll-to-roll manufacturing and the operational stability of organic solar cells (OSCs) in portable and outdoor applications. This paper begins by reviewing the mechanical properties—principally stiffness and brittleness—of pure films of organic semiconductors. It identifies several determinants of the mechanical properties including molecular structures, polymorphism, and microstructure and texture. Next, a discussion of the mechanical properties of polymer:fullerene bulk heterojunction

blends reveals the strong influence of the size and purity of the fullerenes, the effect of processing additives as plasticizers, and the details of molecular mixing—i.e., the extent of intercalation of fullerene molecules between the side chains of the polymer. Mechanical strain in principle affects the photovoltaic output of devices in several ways, from strain-evolved changes in alignment of chains, degree of crystallinity, and orientation of texture, to debonding, cohesive failure, and cracking, which dominate changes in the high-strain regime. These conclusions highlight the importance of mechanical properties and mechanical effects on the viability of OSCs during manufacture and in operational environments. The review—whose focus is on molecular and microstructural determinants of mechanical properties—concludes by suggesting several potential routes to maximize both mechanical resilience and photovoltaic performance for improving the lifetime of devices in the near term and enabling devices that require extreme deformation (i.e., stretchability and ultra-flexibility) in the future.

Broader impacts

Organic solar cells (OSCs) are potentially an inexpensive source of renewable energy that can be manufactured at speeds that dwarf the rate at which wafer-based devices (i.e., silicon) can be fabricated. While low efficiencies of OSCs have historically been regarded as a major roadblock, the performance of this class of printable devices is improving rapidly, and module efficiencies of ten percent now seem possible. The susceptibility of polymer-based active layers to undergo thermally activated phase separation, photochemical damage, and other forms of degradation has motivated large and expanding literature devoted to understanding and improving the long-term stability of modules. Conspicuously absent from the literature, however, is a similar effort directed toward understanding the mechanical properties of organic

semiconductors and their effects on the lifetime of devices against mechanical failure. The principal advantage of OSCs and all printed electronic devices is, nonetheless, roll-to-roll manufacturing on flexible substrates. Manufacturing, installation, and use of these devices will thus require substantial mechanical resilience. Moreover, the ability to make devices on ultrathin plastic sheets—necessary to achieve low production energy for whole modules—requires that the active materials withstand at least some mechanical strain. This article reviews the literature on the mechanical properties of organic semiconductors, the ways in which strain impacts the photovoltaic performance of modules, and what can be done to understand and mitigate these effects. The goal of this review is thus to connect the molecular structure and solid-state microstructure to mechanical properties and mechanical forms of degradation. In addition to increasing the mechanical stability of devices envisioned in the near term, understanding how mechanical resilience and high-performance semiconducting properties can coexist could enable devices for extreme deformation, for example, in portable and wearable applications. Our analysis reveals that there are several potential routes toward co-engineering both mechanical resilience and photovoltaic performance.

1. Motivation

Organic solar cells (OSCs) have achieved benchmarks in the research laboratory that may have seemed out of reach only a decade ago: power conversion efficiencies over 10 percent,[1] projected lifetimes of devices on rigid substrates of over years,[2] power-to-mass ratios of 10 W g^{-1},[3] and projected energy payback times on the order of days.[4] These achievements have been realized, in general, by an approach that uses power conversion efficiency (*PCE*) or some other figure of merit to guide the design and selection of materials and parameters for processing. For

organic solar cells to reach the performance and robustness needed to provide inexpensive power on the scale of gigawatts or—in a best-case scenario—terawatts,[5] significant work remains to be done to translate the gains in the research laboratory toward the production of modules in a roll-to-roll manner.[6] Krebs and coworkers have suggested an alternative approach in which the requirements for manufacturing inform the design of materials.[7] The minimum requirements for low-cost and green[8, 9] materials to be amenable to manufacturing include stability while printing from solution,[10] in air,[11] at low temperatures, from environmentally benign solvents,[12, 13] without vacuum steps,[14] and with tolerance of inhomogeneities in thickness and morphology that appear in printed films.[7, 15] (Fundamental and theoretical studies designed to understand the mechanism of operation, of course, inform all efforts to improve the efficiencies of devices.[16-19]) One aspect of the design of materials that is seldom considered[20, 21]—but that is critical to the stability and lifetime of thin, flexible, lightweight modules destined for outdoor or portable use—is mechanical stability.[22-24] This attribute is generally excluded from an approach that is centered on efficiency,[7] but is included in one that is centered on the requirements for manufacturing and viability under conditions in outdoor[25] and portable environments.[26]

It may seem, because thin films of virtually any material are flexible relative to thicker specimens, that organic semiconductors are already sufficiently compliant for flexible applications and for high yield in roll-to-roll manufacturing. An examination of the modest literature on the mechanical properties of organic semiconductors reveals that their responses to mechanical deformation are highly variable[22, 24, 27-33] (see **Figure 1** for structures referred to in the text, and **Table 1** for a summary of the mechanical properties of pure organic semiconductors and composites). Moreover, good electronic performance—associated with long conjugation lengths and high degrees of crystallinity—seems to correlate with stiffness and brittleness.[24, 28, 33]

Some studies, however, have shown that this correlation is not a fundamental trade-off and that it is, in principle, possible to achieve the "best of both worlds" of mechanical and electronic performance.[27, 29, 34-36] Predicting trends in mechanical properties requires an understanding of the ways in which a molecular structure produces a solid-state microstructure,[28] and how structures at both length scales influence the mechanical and electronic properties of a solid material.[24, 27, 33]

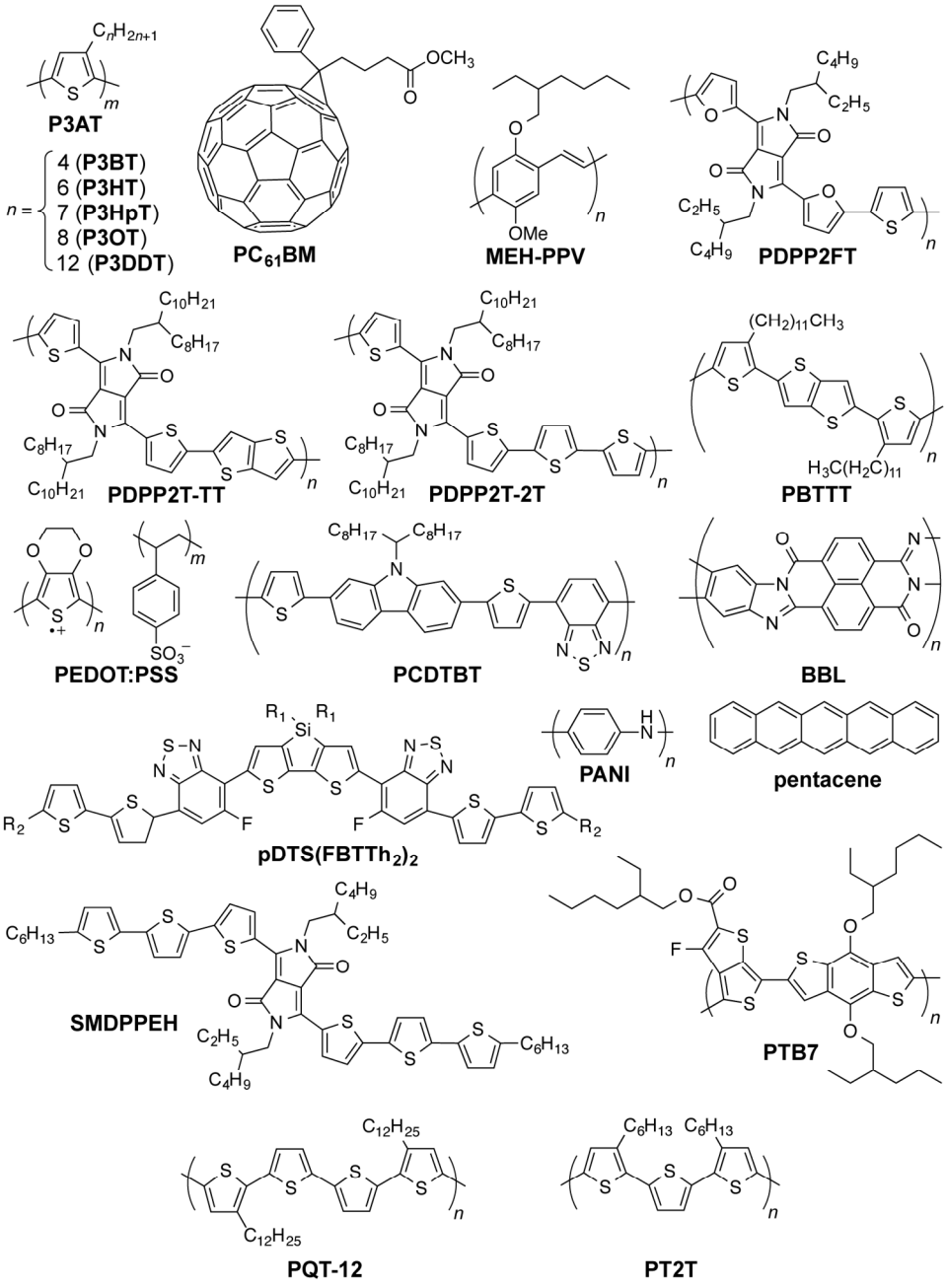

Figure 1. Chemical structures of organic conductors and semiconductors discussed in the text.

Table 1. Tensile moduli (along with crack-onset strains) of all organic electronic materials measured by the buckling technique.

Materials	Notes	Tensile modulus [GPa]	Crack on-set strain [%]	Reference
P3HT	AC	1.33 ± 0.01		32
		1.3		88
		0.92		31
		0.252 ± 0.06	>150	33
		1.09 ± 0.15	9 ± 1.2	28
		0.22 ± 0.03		24
P3HT:PCBM	Ratio 1:0.8, AC	6.02 ± 0.03		32
	Ratio 1:1, AC	4.3		31
	Ratio 1:1, AC	1.97 ± 0.07		131
	Ratio 1:1, AN	2.75 ± 0.09		131
	Ratio 1:0.5, AC	2.02 ± 0.48	3 ± 1.5	28
	Ratio 1:1, AN (ODCB)	~1.74 to 1.97	~2% to >80%	24
P3HT:Fullerene	$PC_{71}BM$ (90%), AC	0.67 ± 0.07		125
	$PC_{71}BM$ (90%), AN	1.76 ± 0.04		125
	$PC_{71}BM$ (90%), AC	2.72 ± 0.40		125
	$PC_{71}BM$ (90%), AN	3.21 ± 0.06		125
	ICBA (99%), AC	3.27 ± 0.86		125
	ICBA (99%), AN	6.53 ± 1.88		125
P3BT	AC	1.87 ± 0.52	6 ± 1.5	28
P3BT:PCBM	Ratio 1:0.5, AC	5.2 ± 0.61	2 ± 0.6	28
P3PT	AC	1.33 ± 0.14		27
P3HpT	AC	0.07 ± 0.01	58	27
	AN	0.13 ± 0.01		131
P3HpT:PCBM	Ratio 1:1, AC	0.61 ± 0.09		131
	Ratio 1:1, AN	1.46 ± 0.16		131
	Ratio 1:1, AN (ODCB)	1.79 ± 0.35		27
P3OT	AC	0.15 ± 0.05	65 ± 2.5	28
P3OT:PCBM	Ratio 1:0.5, AC	0.52 ± 0.16	47 ± 2.1	28
P3DT	AC	0.12 ± 0.4		27
P3DDT	AC	0.16 ± 0.07	47 ± 3.1	28
P3DDT:PCBM	Ratio 1:0.5, AC	0.47 ± 0.17	44 ± 1.4	28
DPPT-TT	AC	0.99		31
DPPT-TT:PCBM	Ratio 1:1, AC	1.4		31
DPPT-2T	AC	0.74		31
DPPT-2T:PCBM	Ratio 1:1, AC	0.84		31
PT2T	AC	1.11 ± 0.19		29
	AN	1.01 ± 0.27		131
PT2T:PCBM	Ratio 1:2, AC	1.6 ± 0.36		29
	Ratio 1:1, AC	2.0 ± 0.36		131
	Ratio 1:1, AN	2.61 ± 0.39		131
PDPP2FT	AC	2.17 ± 0.35		29
PDPP2FT:PCBM	Ratio 1:2, AC	2.76 ± 0.77		29
MEH:PPV	AC	0.119 ± 0.005		131
	AN	0.023 ± 0.001		131
MEH:PPV:PCBM	AC	3.79 ± 0.07		131
	AN	4.92 ± 0.09		131
PBTTT	AC (ODCB)	0.879 ± 0.243	<2.5	33
	AN (ODCB)	1.8 ± 0.345	<2.5	33
	AC	1.8 ± 0.19		131
	AN	2.9 ± 0.30		131
PBTTT:PCBM	AC	3.76 ± 0.8		131
	AN	4.38 ± 0.68		131
PEDOT:PSS		2.26 ± 0.05		32
	5% DMSO, 10% Zonyl	0.03 ± 0.01		71
	5% DMSO, 1% Zonyl	3.14 ± 0.12		71
	5% DMSO, 0.1% Zonyl	7.49 ± 1.5		71
PANI		0.03		32
Pentacene		16.09		32
PCBM	C60	3.06 ± 0.17		24
	C60	6.2		88

† Ratios are reported in weight ratio. Films with thermal annealing treatments are denoted as annealed (AN), while untreated films are denoted as as-cast (AC). Films are spin-coated from chloroform or otherwise noted.

The range over which mechanical properties vary will have significant consequences for the long-term stability of devices, and will thus influence the selection of materials for particular applications. Annealed films of pure PBTTT and composite films of P3HT:PCBM—the *Drosophila* of organic solar cells—crack at strains <2.5% on polydimethylsiloxane (PDMS) substrates under typical processing conditions.[33] Evaporated films of the molecular semiconductor pentacene (and presumably other van der Waals solids) are likely to be more brittle than are films of P3HT:PCBM.[32] Other researchers have noted the importance of understanding the mechanical failure mechanisms.[21] In the report of a Workshop on Key Scientific and Technological Issues for Development of Next-Generation Organic Solar Cells, sponsored by the US National Science Foundation and the Office of Naval Research, researchers asked, "What has been done to prevent solar cells from failing mechanically?"[37] Moreover, in a well-known paper in which researchers deployed roll-to-roll fabricated, OSC-powered, LED lanterns in rural Zambia, one of the principal conclusions was that "…mechanical failure mechanisms were dominant during the field test and therefore these would have to be improved significantly before the photochemical stability of the [semiconducting] polymer becomes a problem."[26] Mechanical stability is of critical importance not only for portable applications—for which accommodation of strain is an operational requirement[38]—but also for roll-to-roll production, transportation, and for utility-scale applications.[7, 25]

In large-scale solar farms and in portable applications, thin organic solar modules will be subject to a range of stresses due to environmental forces.[25] The pressure of wind and the weight of rain and snow will strain the devices to an extent that depends on the compliance and thermal expansion of the encapsulants and support structures. Robust encapsulants and support structures will add significant expense to the modules,[39] and it is thus desirable to use active materials that

can accommodate at least some strain without the need for expensive, rigid supports. Even the thinnest support structures add significantly to the production costs of thin-film PV modules: Anctil et al. calculated that a 130-μm poly(ethyleneterephthalate) (PET) substrate contributes approximately 10% of the embodied energy (along with a roughly equal amount for the encapsulants) of organic modules made using conventional materials, and nearly double that amount in ITO-free devices.[39] One inevitable mode of mechanical deformation that will occur even in the presence of protective layers is thermal expansion and contraction due to diurnal and seasonal variations in temperature. Materials and devices must thus tolerate the extreme conditions in a given geographical area, as well as exhibit resistance to fatigue in the face of cyclic loading due to modest thermal cycling. It is possible that the surface of a highly absorbing device may reach temperatures of 70 °C in the Southwestern US, and a *range* of as much as 100 °C over the lifetime of a device in the Midwest, if one accounts for inevitable extremes in temperatures. One of the goals of the community interested in the mechanical properties of organic semiconductors is thus to mitigate the effects of thermal expansion and contraction on the lifetime and performance of OSCs.

There are a large number of competing technologies in the field of solar photovoltaics. All of these technologies ostensibly have the same goal: achieving the most favorable cost per watt, amortized over the lifetime of the device, for utility-scale installations.[40] Organic solar cells, however, have several characteristics that would be difficult or impossible to replicate in conventional or other thin-film technologies. These characteristics include: semitransparency[41, 42] and tunable color for aesthetic considerations,[43] thermally activated charge transport[44] and possibly increased efficiency at elevated temperature, high-speed manufacturing under ambient conditions,[6, 25] extreme thinness and light weight,[3] and the potential to tolerate high strains

without loss of function.[30, 31] One strategy to hedge against a winner-take-all outcome (if a non-organic PV technology becomes dominant for utility-scale applications) is to focus on areas in which OSCs could "run away" with part of the PV market.[22] Mechanical compliance is the fundamental attribute that provides the basis for all advantages of OSCs.[45] Physical robustness is a prerequisite for fabricating devices on ultrathin substrates, because small forces can produce strains large enough to crack, delaminate, or plastically deform thin films of semiconducting polymers.[3, 46, 47] Moreover, in some portable,[26] wearable,[38] and implantable[48] applications, extreme mechanical compliance[30] and resistance to mechanical failure is at least as important as photochemical[49] and morphological[21] stability.[50-52]

This article reviews the current state of knowledge of the mechanical failure of organic solar cells. The focus is on the ways in which molecular structure influences the microstructure of conjugated materials in the solid state, and how these parameters combine to dictate mechanical properties. The focus on molecular structure and microstructure reflects the expertise of the authors, and we thus invite readers interested in other important aspects of mechanical stability, such as continuum theories of deformation and fracture, to consult references herein.

2. Mechanical properties of organic semiconductors

The factors that ultimately control the mechanical stability of OSCs can be reduced to intermolecular and surface forces present in samples of organic semiconductors and ancillary materials, and how they influence the properties of thin films (mediated by the conditions of processing). The early literature—in the 1980s and early 1990s—contained several studies of the mechanical properties of some of the first-reported conjugated polymers.[53-57] It is apparent, however, that the discovery of the polymer solar cell by Heeger and Wudl,[58] and independently

by Friend,[59] along with the discovery of the organic light-emitting device by Friend,[60] and invention[61] and refinement[62] of the polymer thin-film transistor, shifted the focus from bulk properties—i.e., mechanical properties—familiar to polymer scientists and mechanical engineers, to electronic properties familiar to physicists and electrical engineers. Mechanical properties thus took a back seat to electronic performance, during which time important work was done on improving electronic figures of merit (e.g., power conversion efficiency, *PCE*, in organic solar cells). Much of the success of the field in improving the performance of devices came through the proliferation of the molecular structures accessible by synthetic chemistry.[8, 63-67] Mechanical properties, such as tensile modulus, ductility, fracture toughness, and other parameters of new materials, however, are seldom reported and would be difficult to judge based only on molecular structure. Nevertheless, recent work has attempted to produce some generalities about the ways in which molecular structure and solid-state microstructure influence the mechanical properties of these materials. Far more is known about the mechanical properties of semiconducting polymers than is known about their small-molecule counterparts, and thus Section 2.1 begins with a discussion of the structural determinants of the mechanical properties of pure conjugated polymers.

There is no single figure of merit possessed by an organic semiconductor or composite that will predict the mechanical stability of a whole module: desirable properties will depend largely on the application and on the properties of other materials in the device. The substrate and encapsulant provide structural support, and if the substrate fails mechanically then the device will most likely fail electronically, so it is not necessary that the organic semiconductors provide structural support (e.g., high tensile strength may be desirable, but not if the film fractures at low strains). In general, the active materials should deform with the substrate. That is, they should

have a low modulus and high elastic limit. The strain at which cracks appear in a film on an elastic substrate is often taken as a measure of the ductility of a thin film, but the so-called crack-onset strain is highly dependent on the adhesion between the film and the substrate (poorly adhered films crack at smaller strains than well adhered films of the same modulus).[28] Adhesive[68, 69] and cohesive[23, 52, 70] fracture energies have been proposed to predict the mechanical modes of degradation within the active materials and electrodes in whole modules, and we will return to these figures of merit in more detail in Section 3.2.2. Adhesive energy, however, is sensitive to the order in which layers are deposited,[68, 69] and cohesive energy often depends on thickness.[50] Of all these figures of merit, tensile modulus has the advantages of being easily measured, intrinsic to the material (as opposed to its interaction with a substrate or overlayer), insensitive to thickness for those typically used in devices ($\geq$ 50 nm), and easily relatable (and sometimes predictable) on the basis of chemical structure and microstructure. Additionally, tensile modulus and crack-onset strain (i.e., effective brittleness) are correlated for every system of conjugated polymers in which both quantities are reported in the same paper,[24, 27, 28, 33, 71] and thus a low tensile modulus can be used as a proxy for a favorable response to deformation in mechanically robust applications. Tensile modulus, however, will not predict the mechanical response past the elastic limit, nor will it predict the elastic limit (though we have observed that low tensile modulus is correlated with high elastic limit in P3ATs).[30]

2.1. Mechanical properties of pure organic semiconductors

2.1.1. Conjugated polymers

The basic structural motif of a conjugated polymer—the alternating arrangement of single and double bonds along the backbone[72]—gives rise to the band structure, but also restricts

conformational freedom of unsubstituted conjugated and other rod-like polymers.[73] These materials are thus typically insoluble and rigid. The rigidity of all-sp^2-hybridized materials originally made conjugated polymers attractive for their mechanical strength,[72] which was demonstrated in aligned films of polyacetylene (modulus of 50 GPa and tensile strength of 0.9 GPa)[54] and other structurally simple polymers.[55] For flexible electronic devices, however, tensile strength is less important than is elasticity and toughness,[50] which contributes to the robustness of thin-film devices. The installation of aliphatic side chains on conjugated main chains renders these materials soluble,[64, 74] and also has the effect of increasing the compliance and ductility.[28, 57] Polymers can, however, have similar molecular structures but adopt different microstructures (e.g., polymorphs,[75, 76] textures,[77-79] and degrees of crystallinity[33]) in the solid state, and highly crystalline samples tend to be stiffer and more brittle than samples of the same material that are amorphous or have low crystallinity.[29, 33, 80] The favorable correlation between crystallinity and charge transport on one hand, and the unfavorable correlation between crystallinity and brittleness on the other, is an example of a recurring theme in which charge transport and mechanical properties tend to be in competition.

2.1.2. Experimental determination of the mechanical properties of conjugated polymers

The mechanical properties of conjugated polymers (principally the properties under tensile loading, such as ultimate strength and tensile modulus) have been determined in the past by direct tensile testing[81] and by nanoindentation.[82-84] It is, however, difficult to obtain mechanical data from the geometry that is most relevant to organic optoelectronics—a thin film.[85, 86] Films of organic materials can have thickness-dependent mechanical properties due to unsaturated intermolecular bonds at interfaces (a skin-depth effect)[87] and because of confinement of a plastic

zone at the crack tip during decohesion of layers sandwiched between relatively rigid substrates.[50, 52] The mechanical (and adhesive) properties of organic thin films are thus not necessarily reflective of the properties of samples that are macroscopic in every dimension. Organic films with thicknesses ≤100 nm tend to confound measurements by direct tensile testing because (1) it is difficult to produce and manipulate free-standing thin films and (2) thin areas, inclusions, and other defects can concentrate stress and thus dominate the mechanical response. Nanoindentation has produced useful qualitative and relative data, but the accuracy of the mechanical measurements are limited by the convolution of the effect of the substrate, viscoelastic behavior of the polymer, and the uncertainty of the tip size and contact area of the scanning probes.[83, 84, 86]

The mechanical buckling technique has proven useful in determining the tensile modulus of a range of inorganic and organic thin films,[85, 86 88] and even of individual single-walled carbon nanotubes.[89] The method is based on the buckling instability that gives rise to wrinkles in a relatively rigid film on a relatively compliant substrate under compressive strain.[90, 91] The wavelength of the wrinkling pattern, λ_b, can be related to the tensile modulus of the film, E_f, in terms of the modulus of the substrate, E_s, the thickness of the film, d_f, and the Poisson ratios of the film and substrate, v_f and v_s, in equation 1.[86]

$$E_f = 3E_s\left(\frac{1-v_f^2}{1-v_s^2}\right)\left(\frac{\lambda_b}{2\pi d_f}\right)^3 \qquad (1)$$

In practice, plotting λ_b as a function of d_f for a series of samples (or for a single sample bearing a gradient in thickness) and inserting the slope into equation 1 yields the modulus of the film. The modulus scales with the cube of the slope, and this sensitivity thus requires that the measurement be carried out with strict adherence to established procedures.[86] Poor interfacial adhesion[92] and surface defects—such as pre-existing wrinkles, delamination, and cracking—can produce

apparent buckling wavelengths that produce measurements that deviate significantly from the intrinsic values of the films. **Table 1** is a comprehensive table containing the modulus of every organic electronic material and composite measured by the buckling method.

2.1.3. Influence of alkyl side chains on mechanical properties of conjugated polymers

An analysis of the literature reveals that a critical structural determinant of the mechanical properties of solution-processible conjugated polymers is the alkyl side chain.[27, 28, 57] The role of the side chain in a comb-like polymer in determining its stiffness can be understood intuitively: the longer the alkyl chains (n), the lower the density of load-bearing bonds in the main chain per cross sectional area.[56] Indeed, the fraction of volume occupied by the main chain (versus the side chain) per molecule are 0.31 for butyl side chains and 0.20 for dodecyl chains.[57] Additionally, in polymers with long alkyl side chains, secondary interactions between adjacent main chains are reduced; Wudl and coworkers observed similar effects in another class of comb-like polymers, the poly(alkyl isocyanates).[56] **Figure 2a** plots the tensile modulus vs. the length of the alkyl side chain for a series of poly(3-alkylthiophenes) (P3ATs).[28] The steepest drop-off in modulus occurs between polymers having between six and seven[76] carbon atoms in the side chain, and corresponds to the point at which the glass transition temperature (T_g) drops below ambient temperature (25 °C) with increasing n.[27] The glass transition refers only to the amorphous domains of the polymer, and is always lower than the melting temperature (T_m) of the crystalline domains. The behavior shown in **Figure 2a** suggests the intriguing possibility that P3ATs with $n \geq 7$ might behave as semiconducting thermoplastic elastomers (if the crystallites could be melted without decomposing the polymer). Values of T_g for the most well studied member of this family, P3HT, have been measured to occupy a range of values between 15 to 25 °C.[93, 94] This

proximity to “room temperature” might account for measurements of the modulus that are typical (~1 GPa)[28, 32] or substantially lower (~0.1 GPa).[33] Similar to P3HT, the values T_g for other P3ATs are reported as a range, most likely due to differences in molecular weight, polydispersity, thermal history, and method of measurement.[95, 96] The glass transition of the amorphous domains is thus an important predictor of the mechanical properties of a conjugated polymer, but the percent crystallinity and the order within the crystallites also play important roles.[24]

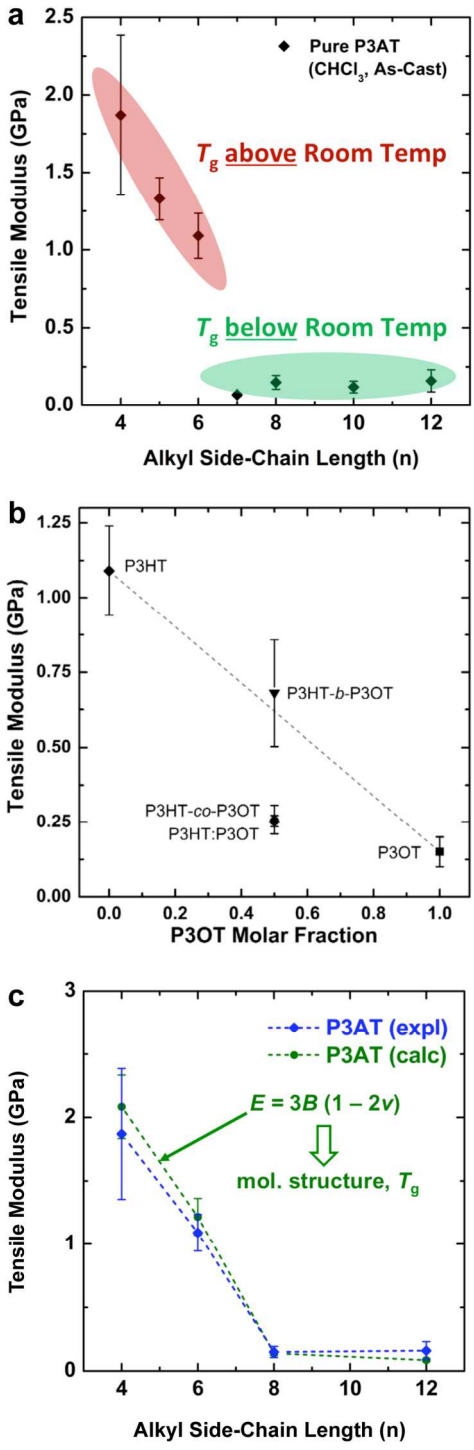

Figure 2. Tensile moduli of poly(3-alkylthiophenes) (P3ATs). (a) Tensile modulus vs. the length of the alkyl side chain (*n*). A sharp drop-off occurs with increasing *n* as the glass transition drops below ambient temperature, from *n* = 6 to *n* = 7. (b) Moduli of three "hybrid" materials with equimolar ratios of hexyl and octyl side chains: a block copolymer (P3HT-*b*-P3OT), a statistical copolymer (P3HT-*co*-P3OT), and a physical blend (P3HT:P3OT). Reproduced with permission from ref.[28]. Copyright 2014, American Chemical Society. (c) Overlay of the experimental and theoretical tensile moduli of P3ATs vs. the length

of the alkyl side chains. Reproduced with permission from ref.[28] Copyright 2014 Wiley-VCH Verlag GmbH & Co. KGaA.

The interesting mechanical behavior of P3ATs in which $6 \leq n \leq 8$ led us to investigate "hybrid" systems, comprising equal molar fractions of hexyl and octyl side chains (**Figure 2b**).[27] These hybrid systems were a physical blend of P3HT and P3OT (P3HT:P3OT), a block copolymer (P3HT-*b*-P3OT), and a statistical copolymer (P3HT-*co*-P3OT). The modulus of the block copolymer sat on a line extrapolated between P3HT and P3OT. This average modulus can be attributed to the covalent connectivity of the relatively stiff P3HT and the relatively plastic P3OT. The modulus of the physical blend, in contrast, sat below the extrapolated modulus, possibly because the P3OT domains—unconstrained by covalent tethering to the P3HT domains—absorbed the strain and thus dominated the mechanical response of the composite material.[27] None of these hybrid materials, however, exhibited as low a tensile modulus as did P3HpT, and the factors governing the combination of high compliance and good photovoltaic properties of this interesting material are still under investigation. It appears, however, that the percent aggregate and the order within the crystalline domains of P3HpT are similar to that of P3HT, while these quantities for P3OT are substantially reduced.

The presence or absence of interdigitation of the side chains of conjugated polymers could be a predictor of the mechanical properties of the solid film.[75] The side chains of the P3ATs generally do not interdigitate,[75] and thus the lamellae within the crystallites should not be as highly registered vertically as in materials in which the side chains do interdigitate (such as PBTTT[33, 66] and PT2T[97]). The decreased number of van der Waals interactions between side chains in non-interdigitated polymers should produce crystallites that are more easily deformable than those in which the side chains are interdigitated. Evidence for interdigitation of the side chains in PBTTT comes by way of a reduction in the (*a*00) lamellar spacing (measured by

GIXD) compared to the spacing predicted by the addition of the lengths of two opposing alkyl side chains in their fully extended conformations.[66] Smaller lamellar spacing thus implies interdigitation. Mechanical measurements of PBTTT by O'Connor et al. are highly correlated with its thermal history and thin-film morphology.[33] As-cast samples of PBTTT, which have small crystallites,[66] exhibited tensile moduli that were half those of annealed films,[33] which exhibited large crystallites (and low amorphous fractions) in an earlier study by AFM.[66] Both the as-cast film and the annealed film were highly brittle, and both cracked at strains <2.5% on PDMS substrates.[33] PT2T (**Figure 1**), a structural analogue of P3HT that differs from P3HT on the basis of the regioisomerism and density of attachment of hexyl side chains (which are incorporated in two of every three monomers for PT2T, and in every monomer for P3HT), forms a solid film in which interdigitation is the preferred packing structure.[97] Interestingly, the tensile modulus of PT2T was similar to that of P3HT when cast under similar conditions.[29]

Different crystalline polymorphs of the same material are expected to have substantially different mechanical properties.[75] For example, the crystalline domains of P3ATs have two known packing structures.[76] Form I is the polymorph found under most conditions. It is characterized by side chains that do not interdigitate. Form II occurs in oligomers of 3-hexylthiophene,[75] and for both P3BT and P3HT, conversion from Form I to Form II can occur by exposure to certain solvent vapors (e.g., carbon disulfide).[98, 99] The defining characteristic of Form II is a shortened lamellar spacing, which is attributed to interdigitation of the side chains.[76] Koch et al. made qualitative observations about the mechanical properties as "somewhat brittle in form II while plastic crystalline behavior was observed for form I," but the mechanical properties were not quantified.[75]

2.1.4. Effect of rigidity of the main chain

The high modulus of unsubstituted conjugated polymers (e.g., polyacetylene), compared to analogous saturated polymers (e.g., polyethylene), is a consequence of at least two effects: (1) the inherent rigidity of an all-sp^2-hybridized main chain[73] and (2) the high polarizability of π bonds compared to σ bonds, which produces a high dispersive component of the van der Waals force, and strong interactions between the main chains.[100] While the effect of structural rigidity on the mechanical properties of a solid film has not been investigated rigorously, a few observations have been made in the literature. First, direct comparison of the tensile moduli of PDPP2T-TT (0.99 GPa) and PDPP2T-2T (0.74 GPa), of similar molecular weight, suggested that the fused thienothiophene (TT) unit lent greater structural rigidity to the polymer than did the biothiophene unit (2T).[31] A reasonable hypothesis is that an increasing proportion of fused rings in the main chain ("ladder-like" character[101]) correlates with increasing modulus of the solid film. A well known ladder polymer, the electron acceptor BBL,[102, 103] exhibited a high modulus of 7.6 GPa by tensile testing.[81] Another interesting effect of rigidity of the main chain is on the orientation of molecular packing in high-aspect-ratio crystallites. In typical conjugated polymers (e.g., P3HT) that form one-dimensional nanostructures, the axis of π-stacking is parallel to the long axis of the nanostructure.[104] For one-dimensional nanobelts of the ladder polymer BBL, however, the molecular axis is parallel to the long axis of the nanostructure.[105] These observations suggest that the mechanical properties of individual molecules could be engineered to produce packing structures in the solid state that optimize charge transport for a given application.

2.1.5. Theoretical predictions of mechanical properties

The mechanical properties of simple conjugated polymers can be predicted with high accuracy using a simple semi-empirical theory first reported by Seitz,[106] and applied to semicrystalline semiconducting polymers for the first time by Tahk et al.[32] Our further application of this technique to conjugated polymers with complex molecular structures has revealed significant deficiencies in this technique,[29] but it is nevertheless remarkable in its ability to predict the tensile moduli of the regioregular P3ATs,[28] and other relatively simple polymers.[106] The accuracy of the technique in obtaining the moduli of some semicrystalline P3ATs is remarkable because it was originally intended to apply to amorphous materials.[106] The technique can be used, at the very least, to screen the structures of materials intended for applications requiring significant mechanical deformation, and to guide the selection of more sophisticated theoretical models.[106] The approach described by Seitz, based on a topological method for correlating molecular structure with bulk properties, is briefly outlined as follows.

The tensile modulus, E_f, of a thin film (or any material under small strains) is related to the bulk modulus (B) and the Poisson ratio (v_f) by equation 2,

$$E_f = 3B(1 - 2v_f) \qquad (\mathbf{2})$$

The bulk modulus is related, through the Lennard-Jones potential, to the cohesive energy (E_{coh}), the van der Waals volume at 0 K (V_0), and the volume at the temperature of interest (V) by equation 3.

$$B \approx 8.23E_{coh}\left[\frac{5V_0^4}{V^5} - \frac{3V_0^2}{V^3}\right] \qquad (\mathbf{3})$$

The cohesive energy can, in turn, be calculated from semi-empirical parameters derived from the bond connectivity indices assigned to each atom in the structure of the monomer, in a method described by Fedors.[107] The bond connectivity indices are parameters that embody the size and

the structure of the monomer as well as the conformational freedom of its bonds. The Poisson ratio is related empirically to the cross-sectional area of the monomer (A), by equation 4.

$$\nu = 0.513 - 2.37 \times 10^6 \sqrt{A} \qquad (\mathbf{4})$$

The area is determined by equation 5,

$$A = \frac{V_\mathrm{w}}{N_\mathrm{A} l_\mathrm{m}} \qquad (\mathbf{5})$$

where V_w is the van der Waals volume and l_m is the length of the monomer. Molecular dimensions are also estimated from the connectivity indices. The closeness of the calculated tensile moduli to those of the experimental values for a series of P3ATs is plotted in **Figure 2c**.[28]

2.1.6. Correlation of microstructure and texture on mechanical properties

The mechanical properties of a polymeric thin film are to a large extent a function of its microstructure.[108] The π-stacking distance, lamellar spacing, crystalline order, molecular orientation, and degree of crystallinity[18] will influence the mechanical properties, and are determined by thermal history,[109] processing conditions,[110, 111] and plastic deformation by strain.[78, 80, 112] Several methods of characterization can be used to correlate microstructure and texture to the mechanical properties for several conjugated polymers and polymer:fullerene blends. These methods are spectroscopic (e.g., the weakly interacting H-aggregate model),[24] imaging-based (e.g., AFM), and those based on synchrotron radiation (e.g., grazing-incidence X-ray diffraction, GIXD).[113]

2.1.7. Spectroscopically determined morphology by the weakly interacting H-aggregate model.

In the seminal paper by Spano and coworkers,[114] the authors showed that the UV-vis spectra of P3HT can be deconvoluted into contributions from the vibronic transitions arising

from the aggregated—i.e., crystalline—phase, which are superimposed with the lower-energy, broad absorption of the amorphous phase (**Figure 3a**). The ratio of the absorption, after taking into account the unequal absorption coefficients of the crystalline and the amorphous domains, can be used as an approximate measure of the percent aggregate (taken to be a percentage of material in well ordered domains). Awartani et al. found a strong correlation between the spectroscopically determined order in P3HT:PCBM films (the percent aggregate and the inverse of the Gaussian linewidths of the vibronic transitions, $1000/\sigma$), the power conversion efficiencies of these blends, and the tensile modulus (**Figure 3b**).[24] The authors found a similar correlation between order and brittleness, as manifested in the crack-onset strain.[24] This observation, along with a similar one that correlated the tensile modulus and brittleness with charge-carrier mobility of P3HT and PBTTT as a function of thermal history,[33] suggests that electronic performance and mechanical compliance are mutually exclusive properties. This is a theme, to which we will return, that represents an opportunity for researchers interested in combining properties—e.g., electrical conductivity and transparency—that seem to be antithetical.[45] Poly(3-heptylthiophene) (P3HpT),[109] whose side chains contain seven carbon atoms, is an example of a material for which brittleness, crystalline order, and photovoltaic efficiency are not correlated.[27] Measurements of both tensile modulus and photovoltaic efficiency in P3HpT suggest that it exhibits the "best of both worlds." (We note, however, that P3HpT:PCBM composites are nearly as stiff as P3HT:PCBM films, presumably due to the stiffening effect of PCBM on the amorphous domains of P3HpT, but a recent trend in the literature is to replace PCBM with polymeric or other small molecule acceptors, which may not increase the stiffness of bulk heterojunction films to the extent that PCBM does.)

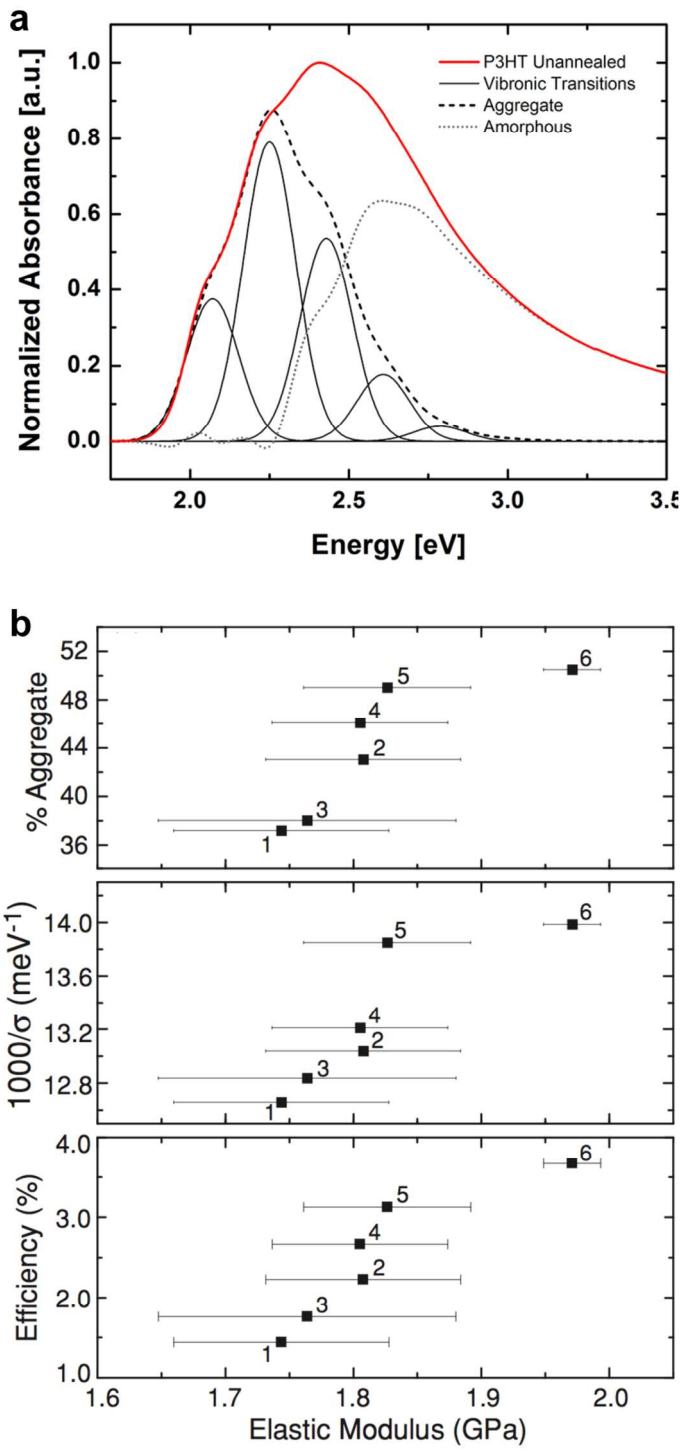

Figure 3. Determination of order within P3HT films by the weakly interacting H-aggregate model. (a) Deconvolution of UV-vis absorption spectrum of P3HT into vibronic peaks associated with aggregated—i.e., crystalline—phases and higher energy absorption of the amorphous domains. Reproduced with permission from ref.[24]. Copyright 2013 Wiley-VCH Verlag GmbH & Co. KGaA.

2.1.8. Morphology of the surface by atomic force microscopy.

The surface of a polymeric thin film can be readily visualized by AFM.[18] Conclusions about the bulk morphology of such films are often drawn, but the morphology visible at the surface of the film does not necessarily resemble that of the bulk.[18] Furthermore, it is difficult to assign apparent differences in phase contrast to specific domains in the film. The usual caveats about artifacts, specific to AFM, also apply. It is important to use a sharp AFM tip to resolve detail, e.g., the nanowire-like morphology observable in low-MW samples of P3HT.[115] Despite its shortcomings, under favorable circumstances, quantities measurable by AFM images can be used to correlate morphology to mechanical properties. For example, PBTTT undergoes a very drastic transition upon thermal annealing, from semicrystalline with small crystallites to a highly crystalline state, in which the well ordered domains are observable by AFM (**Figure 4a**).[66] The annealed, well-ordered state of PBTTT had a substantially increased modulus.[33] For films of P3ATs, roughness is generally correlated to crystallinity, and is thus also loosely correlated to stiffness and ductility (**Figure 4b**). We hasten to add that degree of crystallinity is only one parameter that defines the mechanical properties of a conjugated polymer. Wholly amorphous polymers, such as MEH-PPV and PCDTBT,[116] are in the glassy state at room temperature and can be relatively stiff, in the case of PCDTBT.

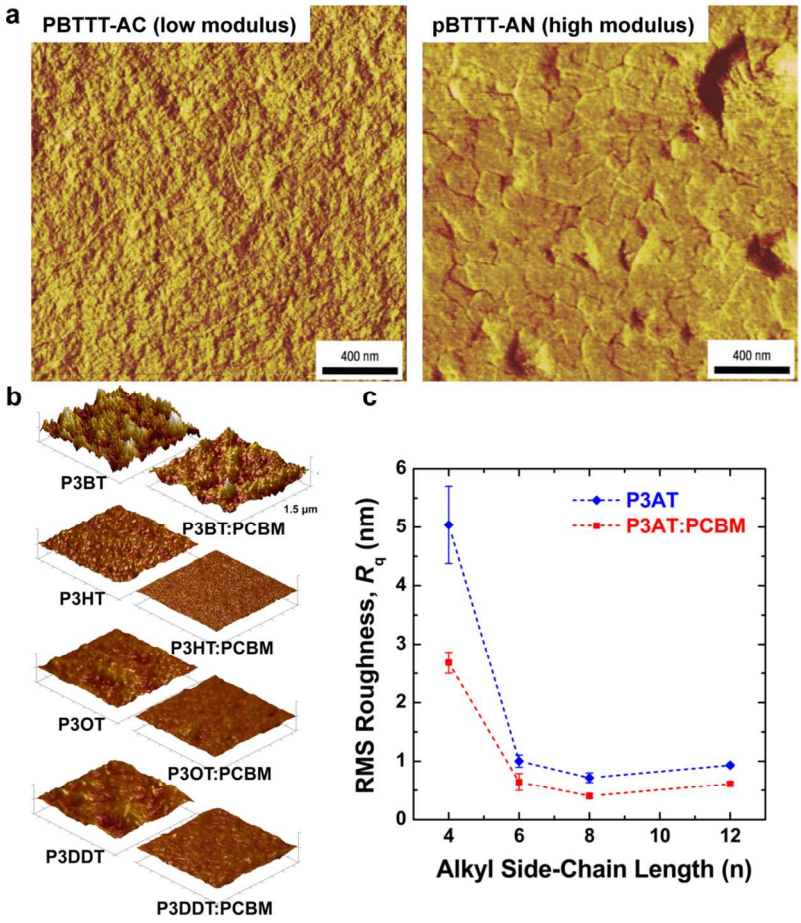

Figure 4. Correlation of surface morphology by atomic force microscopy with mechanical properties. (a) PBTTT undergoes a transition upon thermal annealing from an as-cast form with small crystallites, which is relatively compliant, and a highly crystalline annealed form, which is relatively stiff. Reproduced with permission from ref.[66] Copyright 2006, Nature Publishing Group. (b and c) Roughness is loosely correlated to tensile modulus in P3ATs. Reproduced with permission from ref.[28] Copyright 2014 Wiley-VCH Verlag GmbH & Co. KGaA.

2.1.9. Synchrotron-based X-ray techniques

The most sophisticated approaches to determining the bulk morphology or texture of polymeric thin films involve synchrotron-based methods of characterization. Grazing-incidence X-ray diffraction (GIXD), near-edge X-ray absorption fine structure (NEXAFS), and other techniques provide a wealth of information about microstructure and texture of films of organic semiconductors[18] that can be correlated to mechanical properties. The lamellar spacing can be used to quantify the extent of interdigitation of the side chains in pure polymer phases,[97, 113]

intercalation of fullerenes between the side chains,[23, 117, 118] relative crystallinity (and absolute crystallinity under favorable circumstances),[113] cumulative and non-cumulative disorder,[119] alignment of chains,[78] and can assign the texture as being either edge-on or face-on.[120] Correlations that have been found include the high tensile modulus of PBTTT because of its interdigitated packing structure and highly crystalline morphology when annealed,[33] and the observation that P3HT in its kinetically favorable Form II structure, in which the side chains interdigitate, is relatively brittle.[75]

2.2. Mechanical properties of polymer:fullerene composites

While the mechanical properties of pure polymer films have begun to receive some attention, and conclusions and design rules can be drawn, blending pure polymers with electron acceptors—usually fullerenes—produces effects that can be difficult to predict. The general outcome is that a polymer:PCBM composite is stiffer, more brittle, and has decreased interlayer adhesion than does the pure polymer. The current model that describes the P3HT:PCBM blend comprises (at least) a three-phase system: a crystalline polymer domain, a fullerene-rich domain, and a mixed phase.[19, 121-124] Each phase is expected to contribute to the overall mechanical properties of the film. Processing conditions—e.g., the rate at which the bulk heterojunction forms—affects the order within the crystalline polymer phase, and thus affects the mechanical properties.[24] Intercalation of fullerenes between the side chains of conjugated polymers to form bimolecular crystallites[117, 118] or to prevent crystallization[97] is known to have dramatic effects on the tensile modulus and fracture behavior of polymer:fullerene blends.[23] Other factors, such as the size and purity of the fullerene samples, also play an important role.[125]

2.2.1. Theoretical determination of modulus of composites

Predicting the tensile modulus of polymer:fullerene composites for P3AT:$PC_{61}BM$ is possible using a simple composite theory, which was first applied to these systems by Tahk et al.[32] In this approach, the tensile modulus of the composite is a function of the modulus of the polymer, the Poisson ratio of the film (v, either calculated by equation 4,[28] or more commonly taken as 0.35,[32, 33]), the volume fraction of PCBM in the blend (ϕ_{PCBM}), and the maximum packing fraction of PCBM (ϕ_m, taken as 0.7,[32]).

$$\frac{E_{P3AT:PCBM}}{E_{P3AT}} = \frac{1 + AB\phi_{PCBM}}{1 - B\psi\phi_{PCBM}} \qquad (6)$$

$$A = \frac{7 - 5\nu_{P3AT}}{8 - 10\nu_{P3AT}}, B = \frac{\frac{E_{PCBM}}{E_{P3AT}} - 1}{\frac{E_{PCBM}}{E_{P3AT}} + A}, \psi = 1 + \frac{1 - \phi_m}{\phi_m^2}\phi_{PCBM} \qquad (7)$$

The results from this model are plotted in **Figure 5** on the same set of axes as the experimental data.[28] These composite theories do not account, however, for the ways in which the presence of the fullerene changes the morphology of the polymer phase. In particular, miscibility[123] and intercalation[118] of the PCBM between the side chains of the polymer, can have profound effects on the mechanical properties of films.[23]

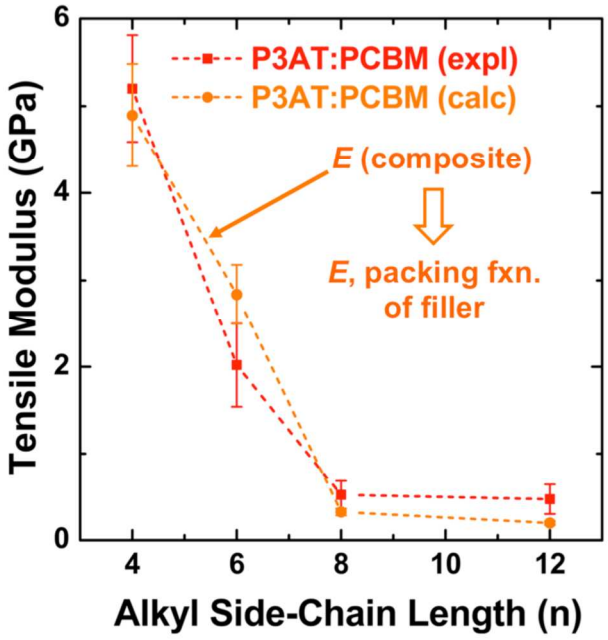

Figure 5. Tensile modulus vs. alkyl side chain length for P3AT:PCBM composites in a ratio of 2:1. The composite theory described in Section 2.2.1 nearly overlaps with the experimental values. Reproduced with permission from ref.[28] Copyright 2014, Wiley-VCH Verlag GmbH & Co. KGaA.

2.2.2. Intercalation and molecular mixing

The original model of the morphology of the polymer:fullerene bulk heterojunction comprised two, generally bicontinuous domains of pure donor and pure acceptor.[126-128] The current three-phase model has been assigned largely by electron tomography[121] (**Figure 6a**) and X-ray analysis.[18, 19, 113, 129] The extent of the mixed phase is governed by the solubility of the fullerene in the amorphous domains of the polymer[122] and by the presence of tie-chains between crystalline domains.[130] The tie chains constrain the expansion of the polymer and thus limit the amount of fullerene that the amorphous domains of the polymer can solubilize.[130] Regiorandom P3HT is completely amorphous and can disperse PCBM at any concentration.[130] The mixing is also dependent on the details of the molecular packing (i.e., the ability of fullerenes to occupy free volume between side chains of the polymer).[118] For example, PT2T is a type of polythiophene that is derived from a tail-to-tail coupled bithiophene bearing hexyl chains and an

unsubstituted thiophene ring (**Figure 6c**).[97] The polymer therefore contains a notch (i.e., the absence of an alkyl chain) every third repeat unit. This structural motif encourages the formation of crystalline domains in which the hexyl chains of adjacent polymer chains interdigitate.[97] Favorable positions of the frontier molecular orbitals suggest that blending this material with PCBM would produce an OPV effect that is possibly greater than that of P3HT:PCBM.[97] In the PT2T composite, however, the fullerene molecules sit in the notch, and thus prevent interdigitation of the side chains of adjacent polymer chains.[97] Thermal annealing does not recover the crystalline microstructure of the pure polymer, and the absence of pure polymer and pure fullerene phases have a disastrous effect on the power conversion efficiency of PT2T:PCBM blends.[97] Intercalation of fullerenes between the side chains is also the basis of the high ratio of fullerenes needed to achieve high efficiencies in blends of PBTTT and PCBM,[117] and probably also MDMO-PPV and PCBM;[118] that is, the weight percentage of fullerenes must surpass some threshold value, beyond which the crystalline phase cannot accommodate additional fullerene molecules. Pure or substantially enriched domains of fullerenes are required for high efficiency. Thus, blends of PBTTT and MDMO-PPV and PCBM, for example, are typically optimized with ratios of polymer to fullerene around 1:4.[118]

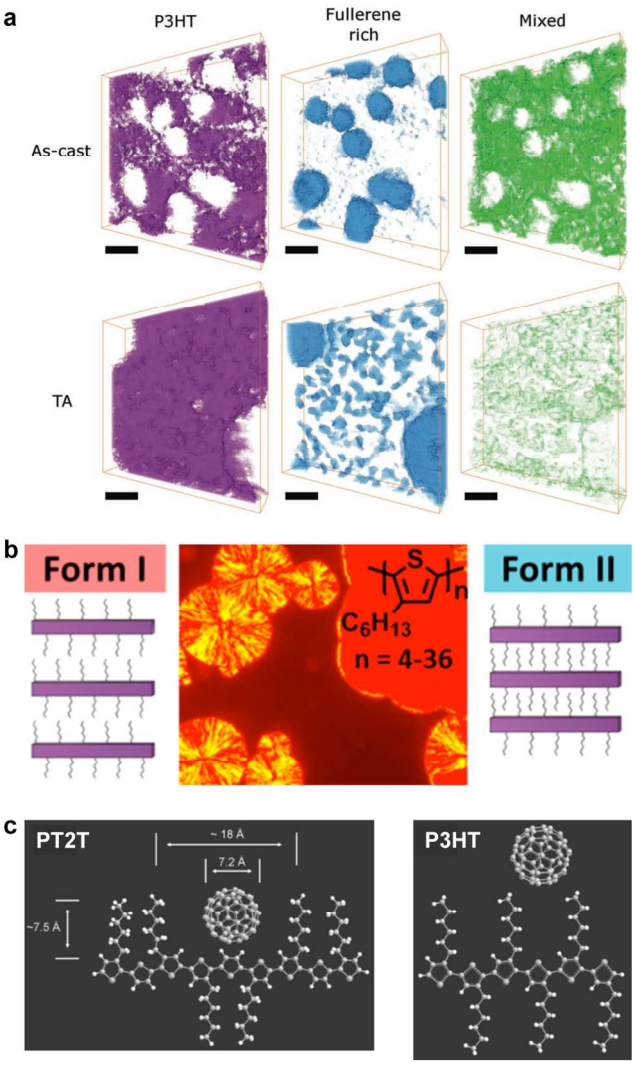

Figure 6. Morphology and packing of organic semiconductor films. (a) Electron tomography using endohedral fullerenes reveals a three-phase system comprising polymer- and fullerene- rich phases, and a mixed phase, which is substantially reduced by thermal annealing. Reproduced with permission from ref.[121] Copyright 2013, Wiley-VCH Verlag GmbH & Co. KGaA. (b) Two crystalline polymorphs of P3HT exist, a thermodynamically favored Form I (spherulites), in which the side chains do not interdigitate, and a kinetically favored Form II (solid red phase), in which they do. Form II is expected to have a greater modulus and higher brittleness than does Form I. Reproduced with permission from ref.[75] Copyright 2013, American Chemical Society. (c) Schematic drawings of PT2T and P3HT, and the hypothesized way in which fullerene molecules can fit between the side chains of PT2T, but not P3HT. Reproduced with permission from ref.[97] Copyright 2007, Wiley-VCH Verlag GmbH & Co. KGaA.

The mechanical properties of polymer:fullerene blends were previously reported to be intimately related to the details of molecular mixing.[23] The tensile moduli of most P3AT:fullerene blends are a factor of 3-5 greater than those of the neat polymers.[28, 32] The typical

rationale for the increased modulus of P3AT:PCBM relative to the neat polymer is the stiffness of the fullerene-rich phase.[28, 32] **Figure 7a** plots the factor by which selected polymer:fullerene composites are greater than that of the neat polymer both before and after annealing. The salient example is P3HpT:PCBM (factor of 7 greater than neat P3HpT).[131] As discussed in Section 2.1.3, P3HpT is the P3AT that maximizes mechanical compliance and electronic performance. Differential compliance and ductility of the P3ATs is largely a function of the fluidity of the amorphous domains at room temperature.[27] In a P3AT:fullerene composite, however, the current model predicts the absence of pure amorphous domains of P3ATs,[130] and thus we conclude that the presence of fullerenes produce stiffened mixed domains, which dominate the mechanical properties of the blend.

The dominance by the stiffened mixed domains on the mechanical properties of polymer:fullerene blends was observable not only in blends with P3ATs, which do not allow fullerene intercalation, but also in other polythiophenes which do allow fullerene intercalation. **Figure 7b** plots the tensile modulus of selected polymer:fullerene blends against the tensile modulus of the neat polymers. Interestingly, for these polythiophenes, there is a linear correlation between the tensile moduli of the neat polymers and the polymer:fullerene blends. This linear correlation suggests that the effects of molecular mixing play a relatively small role in the tensile modulus of polymer:fullerene blends. A striking example is PT2T:PCBM. The neat polymer is relatively highly aggregated due to the interdigitation of the alkyl side chains, though the modulus is similar to that of neat P3HT (~1 GPa, depending on batch-to-batch variability).[28, 29] Blending with PCBM, however, destroys the aggregate microstructure of PT2T. Remarkably, the tensile modulus of even a 1:1 blend of PT2T:PCBM is similar to that of P3HT:PCBM, despite the completely different microstructures. The mechanical properties of bulk heterojunction

composites—due to the complex nature of the blend, which has at least three phases—can vary widely, and offer interesting opportunities for studying nanocomposite materials.

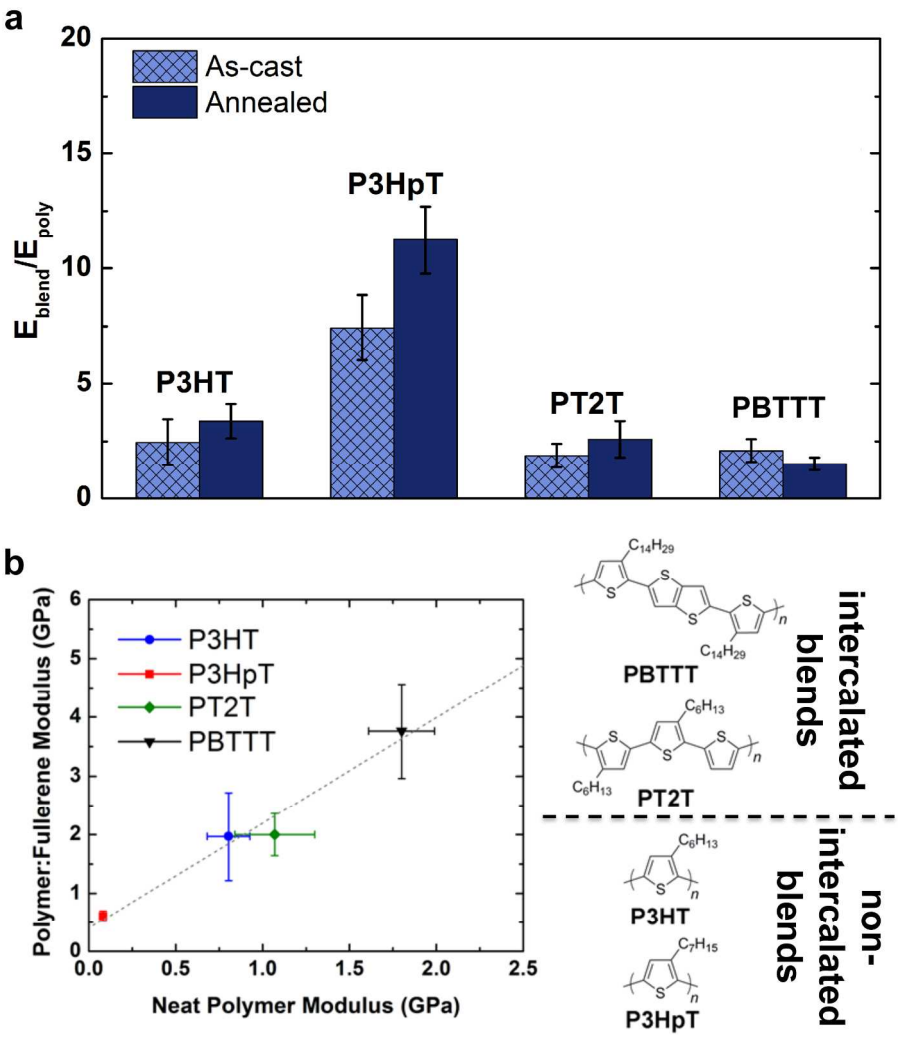

Figure 7. Effect of molecular mixing on the stiffness of polythiophenes. (a) A plot of the modulus of a polymer:fullerene blend vs. the modulus of the neat polymer reveals that the presence of fullerenes have a stiffening effect on the neat polymer; the correlation, however, implies that the details of molecular mixing—i.e., whether or not the fullerenes intercalate between the side chains of the polymer—have a relatively small effect, at least for the materials examined in this study. (b) Plot showing the factor by which a 1:1 blend of polymer and PCBM is greater in modulus than is the neat polymer in both annealed an unannealed forms.

2.2.3. Purity of fullerene samples

Fullerenes are the most popular electron acceptor in organic photovoltaics because of their high charge-carrier mobilities[132] and their spherical (or quasi-spherical) shapes, which permit them to accept electrons from any direction.[133] There are, however, several disadvantages to fullerenes, including cost,[4] embodied energy,[134] possible environmental degradation,[135] and the potential for toxicity. These drawbacks have motivated researchers to explore alternatives to fullerenes[136] to mitigate environmental concerns, or investigate less pure samples of fullerenes to reduce the cost and embodied energy. We undertook a study to understand the effect of the size and purity of the fullerene on the tensile modulus and crack-onset strain of P3HT:PCBM composites using four different samples of derivatized fullerenes: $PC_{61}BM$ (99%), $PC_{61}BM$ technical grade (90% $PC_{61}BM$, 10% $PC_{71}BM$), $PC_{71}BM$ (99%), and $PC_{71}BM$ technical grade (90% $PC_{71}BM$, 10% $PC_{61}BM$). The purer films were stiffer, but the less pure samples produced devices that were only somewhat—but not catastrophically—less efficient than those made from the purest samples (5% degradation in *PCE* for $PC_{71}BM$, and 19% degradation for $PC_{61}BM$.[125] These effects were attributed to the propensity of the fullerene with higher purity to form larger crystalline domains. A slight increase in order of the polymer phase with increasing purity of the fullerene was also observed through UV-vis spectra as analyzed by the weakly interacting H-aggregate model.[125] This study suggests that the use of lower-purity fullerenes may substantially reduce the cost and production energy of organic solar cells, and also increase the compliance and environmental stability of devices (**Figure 8**).[125]

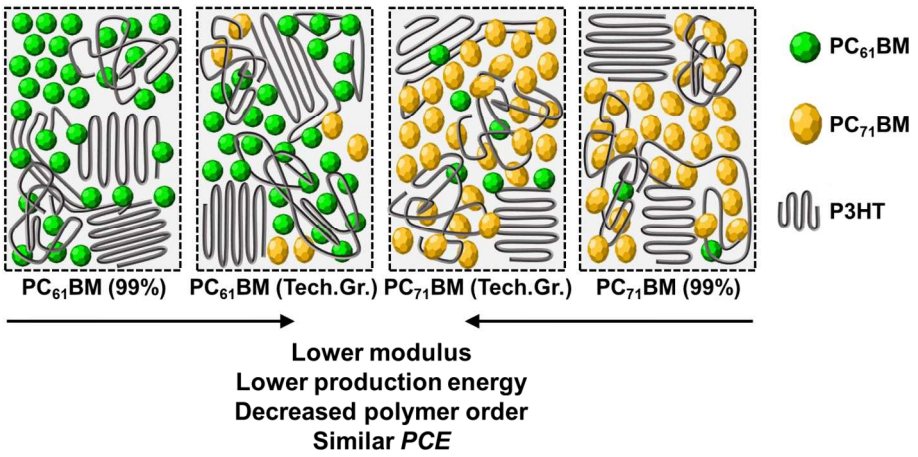

Figure 8. Schematic summary of the effect of purity of fullerenes on the stiffness of P3HT:PCBM blends for $PC_{61}BM$ and $PC_{71}BM$. "Purity" refers to the extent of separation of C_{60} and C_{70} derivatives, where technical grade (Tech. Gr.) contains ≤10% fullerenes of the other size. The results suggest that it is possible to increase the compliance of polymer:fullerene blends while decreasing the purity of the fullerenes to decrease the embodied energy (and therefore the cost).

2.2.4. Effect of additives and plasticizers

High-boiling additives are often included in bulk heterojunction films to increase the performance of polymer:fullerene blends and PEDOT:PSS films by improving the morphology.[137, 138] Small-molecule additives in polymer engineering often have the effect of plasticizers. Plasticizers increase the free volume within samples of solid polymers, and lower the T_g and the tensile modulus. Common additives, such as 1,8-dithiooctane and 1,8-diiodooctane (DIO),[137, 138] have been used for certain bulk heterojunctions comprising low-bandgap polymers blended with PCBM to improve their performance. Graham et al. found that PDMS, often used as a lubricant in the syringes used to dispense polymer "inks" for spin-coating, is also associated with generating a favorable morphology and increased efficiency in solar cells based on solution-processed small molecules.[139] Using P3HT:PCBM as a model system, we found a plasticizing effect for both DIO (69% decrease in tensile modulus) and PDMS (28% decrease), using concentrations typically used in the literature.[28] It is not yet known

whether the decrease in modulus can be attributed to a typical plasticizing effect (i.e., increasing the free volume) or by a change in microstructure that affects the mechanical properties.

Additives and cosolvents are essentially always used in solution-processed films of PEDOT:PSS,[140, 141] and these adjuncts have effects on the modulus (**Figure 9a**) and ductility (**Figure 9b**),[71] along with effects on the sheet resistance (**Figure 9c**),[140] some of which are already known.[142] High-boiling liquids and polar additives, such as dimethylsulfoxide (DMSO) and sorbitol, are associated with increasing the size of the conductive PEDOT-rich grains, and thus increasing the conductivity of the film.[143, 144] Zonyl fluorosurfactant (now called Capstone by DuPont) is used to enable wetting of aqueous dispersions of PEDOT:PSS on hydrophobic plastic substrates,[140, 145] or on the hydrophobic surface of the bulk heterojunction film in the inverted architecture.[146] Poly(ethyleneimine) (PEI),[147] and other amine-containing polymers and small molecules,[148, 149] is used to lower the work function of PEDOT:PSS to permit its use as the cathode (as well as the anode) in all-organic devices. While the use of a thin-layer of PEI seems to have a stiffening effect, Zonyl, when present in the ink in concentrations up to 10%, has a very strong plasticizing effect.[71] It seems, thus, that additives may serve a dual purpose: as cosolvents for one or more components of the bulk heterojunction, and as plasticizers for increased mechanical stability. Interestingly, the concentration of DMSO in the ink of 5%, which produced the most conductive films when the concentration of Zonyl was kept constant, also produced films of greater stiffness and brittleness.[71] The interconnected morphology that supports good charge transport may thus embrittle the films, but this effect can be mitigated by adding Zonyl (or perhaps another surfactant) without degrading the electronic performance substantially.

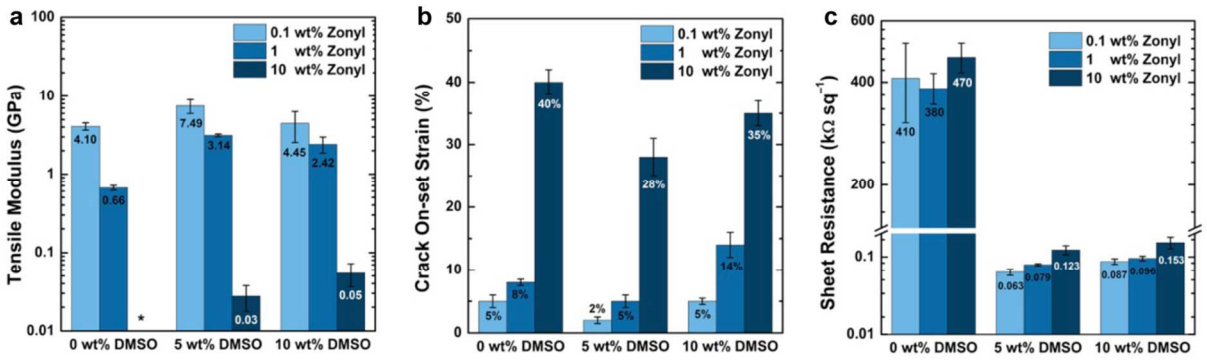

Figure 9. Effect of common additives, Zonyl fluorosurfactant and DMSO, on the (a) tensile modulus, (b) crack-onset strain, and (c) sheet resistance of the ubiquitous transparent conductive polymer, PEDOT:PSS.

2.2.5. Small molecules and oligomers

Compared to their polymeric counterparts, solution-processed small molecules offer advantages of monodispersity and increased overall purity, a greater tendency to produce highly crystalline microstructures, and low cost and low production energy. The power conversion efficiencies of devices with active layers based on small-molecule:fullerene blends are nearly as high as the typical polymer:fullerene system.[150] It may be, however, that the highly crystalline morphology of π-conjugated small molecule films also renders them stiff and brittle. The transition from polymer to oligomeric to small-molecule can coincide with a transition between polymorphs, which can have different mechanical properties. Koch et al., as mentioned in Section 2.1.3, found that oligo(3-hexylthiophene) (degree of polymerization = 4 – 36) exhibited the kinetically favored crystalline polymorph—"Form II"—in which the side chains interdigitated, and underwent a qualitative increase in stiffness.[75] The forms could be interconverted by appropriate treatments, but Form II was generally favored for the shorter oligomers. There is far less information available on the mechanical properties of small-molecule semiconductors than there is about polymeric ones. Films of evaporated pentacene, in addition to having an extraordinarily high tensile modulus of 15 GPa, also exhibited substantial cracking

when transferred to a PDMS substrate for analysis by the buckling methodology.[32] Preliminary observations by our group on solution-processible, small-molecule semiconductors, TIPS-pentacene, SMDPPEH, and pDTS($FBTTh_2$)$_2$, suggest that these van der Waals solids are characteristically brittle. Attempts to measure the moduli and crack-onset strain on PDMS substrates have thus far been unsuccessful, because of cracking of the films during the process of transferring from passivated glass or silicon to PDMS. In high-modulus materials that were eventually measured successfully, this behavior correlated with high stiffness and brittleness, as in P3BT:PCBM.[28] There is, however, a dearth of literature on the mechanical properties of small-molecule films, and definitive statements about the mechanical stability of devices based on solution-processed small molecules cannot be made.

2.2.6. Are mechanical and electronic figures of merit mutually exclusive?

Analyses of several organic conductors, semiconductors, and composites have suggested that good electronic properties—as manifested in conductivity, charge-carrier mobility, and photovoltaic efficiency—and mechanical properties (i.e., elasticity and ductility) are antithetical.[24, 151] Systems in which this competition was observed include P3ATs with side chains having an even number of carbon atoms,[28] P3HT:PCBM films dried at different rates,[24] annealed and unannealed PBTTT,[33] and PEDOT:PSS deposited from inks containing different amounts of DMSO.[71] Recent studies, however, have shown possible routes toward systems that exhibit substantial compliance along with high photovoltaic efficiency. For example, P3HpT has a vibronic structure (as seen in the UV-vis absorption spectrum) that nearly overlaps with that of P3HT, which indicates a similar percentage of aggregate and a similar level of order within the aggregate. Moreover, P3HpT exhibits photovoltaic parameters in blends with PCBM that are

similar to those of the standard (and more brittle) material, P3HT.[27] The amorphous phase in P3HpT is mobile at room temperature, however, while the amorphous phase in P3HT is glassy. The similar electronic performance thus seems to be a manifestation of the degree of crystallinity and the order within the crystalline domains, while the differential mechanical properties are dominated by the amorphous domains. These observations point to a design rule, valid at minimum for semicrystalline materials, for organic semiconductors that are at once high-performance and highly compliant. Another route toward films exhibiting the best of both worlds is plasticization of the active materials by additives—such as DIO and PDMS for semiconductors, and Zonyl for PEDOT:PSS—that are already known to increase the electronic figures of merit.[28] Other approaches, such as covalent incorporation of flexible units (e.g., polyethylene blocks[34] or oligoethylene glycol side chains[152]) may provide further routes toward tailoring the mechanical properties of bulk heterojunctions of high-performance conjugated polymers. Intentional reduction in crystallinity by introducing random units in a polymeric backbone represents another possible method to achieve good photovoltaic performance and high elasticity,[29] as does substitution of fused rings in the main chain of a polymer (e.g., thienothiophene) for isolated rings (e.g., bithiophene),[31] and tailoring the rate at which the bulk heterojunction forms.[24] **Figure 10** shows a plot of power conversion efficiency vs. tensile modulus for six samples of polythiophene. Materials occupying the top-left quadrant in such a plot are potential candidates for mechanically stable solar cells (e.g., P3HpT), or embody rules that will inform the design of high-performance materials in the future.

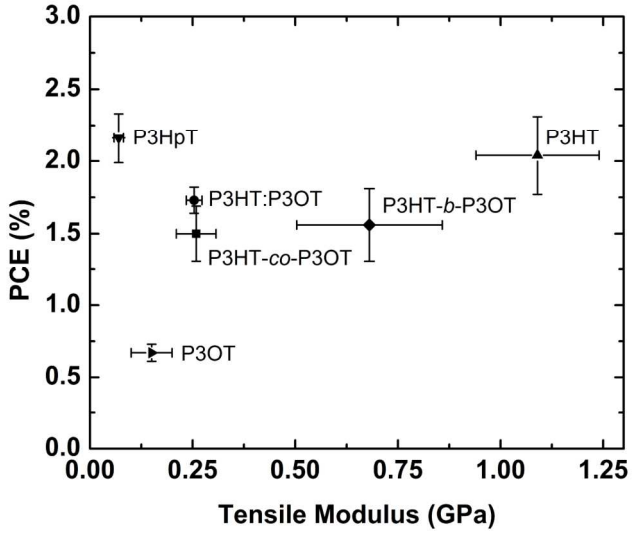

Figure 10. Power conversion efficiency (*PCE*) of polymer:fullerene blends vs. tensile modulus of the pure poly(3-alkylthiophenes): P3HT, P3OT, a physical blend of the two (P3HT:P3OT), a block copolymer (P3HT-*b*-P3OT), a random copolymer (P3HT-*co*-P3OT), and P3HpT. Materials occupying the top-left quadrant (e.g., P3HpT) in principle exhibit a favorable combination of mechanical compliance and photovoltaic performance. Reproduced with permission from ref.[27] Copyright 2014 American Chemical Society.

3. Behavior of materials and devices under strain

All thin-film technologies are susceptible to damage by environmental forces. If changes in the photovoltaic output of devices upon imposition of mechanical stress are not prevented, they should at least be anticipated, so that their effects can be mitigated downstream. We divide the response to strain into two regimes: (1) pre-catastrophic failure and (2) catastrophic failure. The behavior in the first regime, characterized by small-strains (prior to cracking or delamination that produces substantial loss of function) is in principle affected by elastic or plastic deformation of the active materials and contacts. Deformation of the materials continues throughout the second regime, but the photovoltaic output is dominated instead by cracking of the active materials and contacts, failure of the barrier films, and short-circuiting of the electrodes. We define catastrophic failure as occurring when the device loses most or all of its

photovoltaic efficiency. This section also discusses the factors that control interfacial debonding, cracking, and the molecular and environmental determinants of this type of failure.

3.1. Pre-catastrophic failure behavior

This section reviews the evolution in photovoltaic properties in response to strain-evolved microstructures, change in interfacial energies, and the formation of small cracks. The defining characteristic of this regime is that the photovoltaic properties remain generally intact. Many of the strain-evolved changes in microstructure observed in some conjugated polymers—alignment of chains,[78] change in texture from edge-on to face-on,[78, 79] and increased degree of crystallinity[78]—might actually increase the photovoltaic performance of devices under some circumstances.

3.1.1. Strain-evolved microstructure of organic semiconductors.

Charge transport in organic semiconductors is intimately linked to solid-state packing structure,[44] which is perturbed when an active material is strained (**Figure 11**). It is clear, thus, that even the smallest applied strains will change the photovoltaic response of the active material. Strained microstructures do not always have deleterious consequences on the electronic output. For example, Giri et al. found that crystalline films of TIPS-pentacene could exhibit metastable polymorphs with shortened π-stacking distances and thus increased charge-carrier mobility in field-effect transistors.[153] Some of these polymorphs, which are accessible by changing the speed of solution-shearing, are applicable to large-area coverage.[154] Furthermore, the direct application of compressive strain has been shown to increase the mobilities in films of pentacene and tetracene, where the photoconductivity of the crystals increased linearly with

applied hydrostatic pressure.[155] Zinc octakis(β-decoxyethyl)porphyrin films have also exhibited a strong correlation between the increase in compressive strains and a higher photoconductivity, when pressures using a micro tip were applied.[156] The authors attributed these effects to a compression of the π-stacking axis and better overlap of the molecular orbital wavefunctions.

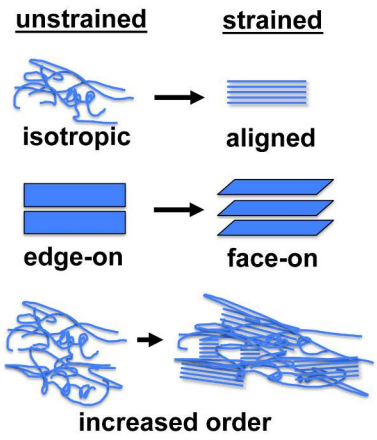

Figure 11. Strain-evolved changes in microstructure shown to occur in polythiophenes. (Top) Tensile strain aligns chains, (middle) affects a reorientation in texture from principally edge-on to face-on, and (bottom) increases the overall percent aggregate.

The most well known effect of tensile strain on a conjugated polymer is alignment of the chains along the strained axis. This effect has been known since early work on conjugated polymers, and is responsible for the extraordinarily high tensile strength of uniaxially aligned polyacetylene.[53, 54] Drawn films of P3HT exhibit highly anisotropic hole mobility, which has been noted by Vijay et al.[112] and O'Connor et al.[78] These studies highlight the importance of along-chain transport in the overall ability of a film to transport charge. This fact was reinforced in a paper by Heeger and coworkers, in which low-bandgap polymers aligned in nanoimprinted grooves exhibited among the highest charge-carrier mobilities reported to date.[157] Aligned films also exhibit polarization-dependent absorption, because of the orientation of the π-π* transition, which is perpendicular to the molecular axis.[158] Awartani et al. has shown substantial

birefringence in stretch-aligned bulk heterojunction films, and thus organic solar cells with polarization-dependent absorption and efficiency.[80] The increase in charge-carrier mobility induced by stretch aligning may benefit field-effect transistors, but the anisotropy is in the wrong direction to benefit organic solar cells, in which charges are transported through the thickness of a film.

A secondary effect of strain on the microstructure of conjugated polymer films, as seen in P3HT, is on the texture. O'Connor et al. noted that strain produced realignment of the π system of the molecules from predominantly edge-on (regarded as the preferred orientation for P3ATs and other conjugated polymers) to largely face-on.[78, 79] The latter orientation may be favorable for OSCs. O'Connor, DeLongchamp, and coworkers have observed this effect in P3HT films under both uniaxial[78] and biaxial[79] deformation. The mechanism and fundamental basis for this realignment remains an interesting and important question for further inquiry, and has implications for the photovoltaic output of devices under strain. It suggests that mechanical strain might actually improve power conversion efficiencies of devices under some circumstances.

A third effect of strain, observed by increases in the intensities of the vibronic transitions of P3ATs, is an increase in the percent crystalline aggregate within the film.[78] This strain-evolved microstructural change could, in principle, produce greater photovoltaic performance, as percent aggregate in the polymer phase is correlated with increased efficiency in P3HT:PCBM devices.[24] While such increases in crystalline order produced by other means—i.e., thermal annealing,[159] solvent-vapor annealing,[160] and slowness of evaporation of the solvent during solution casting[24]—are generally correlated with increases in *PCE*; in a solar cell, tensile strain has possibly detrimental effects on the other components of the device, such as the substrates, interfaces, barrier films, and electrodes, which make it difficult to isolate the effects of strain

itself on the overall properties of the device.[31] **Figure 12a** and **12b** shows the evolution in photovoltaic properties with tensile strain for two types of devices fabricated on PDMS substrates, one based on P3HT:PCBM, and the other based on PDPP2T-TT:PCBM, from 0 to 20% strain.[31] The apparent increase in V_{OC} with small strains for the brittle P3HT:PCBM was attributed to fracturing of the oxide "skin" that forms on the liquid eutectic gallium-indium (EGaIn) cathode—used because it is stretchable—when extruded in air. The same effect is observed if the EGaIn is extruded in air, placed in the glovebox, and then agitated with a wooden applicator, but the effect disappears when the EGaIn is extruded in a nitrogen atmosphere. The effect is more pronounced for P3HT:PCBM than it is for PDPP2T-TT:PCBM, because the former bulk heterojunction is more brittle, and the opening and closing of cracks in the active layer perturb the top electrode to a greater extent. This experiment highlights the difficulty in isolating the effects of the change in microstructure of the active materials from the detrimental effects on the electrodes and other materials.

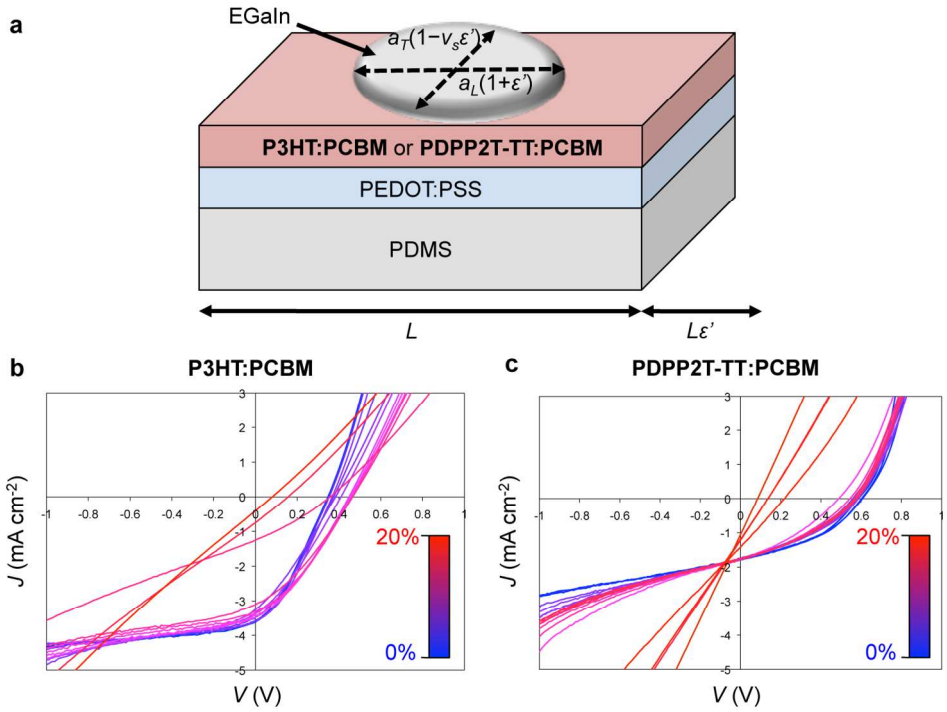

Figure 12. Evolution in photovoltaic output with tensile strain, ε. (a) Schematic diagram of a stretchable device. (b) Current density vs. voltage for a P3HT:PCBM device from 0% to 20% strain. (c) A similar plot for a PDPP2T-TT:PCBM device. Current densities were calculated using the area of the footprint of the drop of eutectic gallium indium (EGaIn), which deformed with strain, by the equation $A(\varepsilon') = \pi a_L(1+\varepsilon')a_T(1-v_S\varepsilon')$, where $\varepsilon' = \varepsilon/100\%$, a_L and a_T are the longitudinal and transverse semi-major axes, and v_S is the Poisson ratio of PDMS (and assumed to be constant within the relatively small range of strains, between 0 and 20%.) Reproduced with permission from ref.[31] Copyright 2012, Elsevier.

Global strains, applied to whole devices, can manifest as damage at interfaces. While the effects of pre-catastrophic bending strains on interfaces have not been rigorously determined for organic solar cells, Sokolov et al. has performed relevant studies on field-effect transistors.[161] The authors' principal conclusion was that the strains applied to these transistors changed the alignment of polymer chains and altered the field-effect mobility of the strained devices due to reorientation of the surface dipoles.[161] Poor interfacial adhesion can produce cracks at sites of local delamination that propagate through multiple layers in the device.[30, 142] Adhesion promoters can reduce this effect substantially, as has been observed for PEDOT:PSS,[30, 142] which behaves as a prime coat that increases adhesion of bulk heterojunction films to hydrophobic substrates.

Lu et al. observed a similar effect in films of copper on polyimide substrates, which could be stretched up to 50%, without cracking, if a chromium adhesion layer was used.[162]

3.1.2. Pre-catastrophic cracking under tensile strain.

There are scenarios in which lateral cracks that appear on the surface of the active material would not lead to catastrophic failure in a device. One can imagine, for example, that a solar cell that cracks without shorting of the electrodes might behave like many smaller solar cells connected in parallel. In fact, Chortos et al. showed that microcracked organic semiconductors functioned normally while strained in stretchable field-effect transistors.[163] In principle, cracking of an electrode would increase the sheet resistance of the contact, which would manifest in increased series resistance, and would, in turn, reduce the fill factor and short-circuit current. Cracks and thin areas in the active layer could produce shunts and lowered parallel (i.e., shunt) resistance, and ultimately decrease the fill factor and open-circuit voltage. These qualitative features are consistent with the behavior of a device with the architecture PDMS/PEDOT:PSS/PDPPT2T-TT:PCBM/EGaIn (**Figure 12c**).[31] As the applied strain approaches 20%, the *J–V* curve resembles a short circuit. In contrast to the examples shown in **Figure 12**, which show the evolution in photovoltaic output with strain due to cracks that appear in the surface of the film, there have not been any studies in which interfacial debonding or cohesive failure were explicitly identified as the origin of failure. One intriguing possibility is that some organic semiconductors might undergo stimulus-responsive healing or repair after damage. It has become clear, for example, that fullerene molecules are highly mobile within the amorphous domains of P3AT films, and can diffuse across interfaces of laminated films.[123, 124] Kahn and coworkers have reported lamination of conjugated polymer films by transfer printing,

and while the laminated film was reported to be essentially identical to a single film with respect to charge transport, the mechanical properties of the welded interface—in particular, the cohesion—has not been characterized.[164, 165]

3.2. Catastrophic fracture

In contrast to Section 3.1.1, which dealt largely with the theoretical effects of strain-evolved changes in microstructure on the photovoltaic properties, the effects of cracking are easily seen in plots of current density vs. voltage, and are nearly always deleterious.[31] The detail to which these effects are characterized in the literature is, however, not fine-grained. In general, bending studies are performed to illustrate the superior mechanical flexibility of one material (e.g., the transparent electrode) over a control device that uses a conventional material (e.g., ITO, though the mechanism by which ITO itself degrades under strain is an active area of research[166]).[167] Degradation of function is attributed to cracking within the control device, however, strain is almost never estimated based on the bending radius and thickness of the substrate, and the specific ways in which the damage manifests in the degraded *J–V* plots are generally not identified. This section is subdivided on the basis of the relative orientation of the strain to the plane of the device: (1) strain applied parallel to the device plane that generally produces cracking and cracking-induced delamination in one or more layers,[31, 145] and (2) strain applied normal to the device plane, which is associated with cohesive and adhesive failure of the thin films that make up the device.

3.2.1. Strain applied parallel to device plane

Strain occurs within the plane of the device when stretched or bent (the strain is tensile on the convex surfaces above the neutral plane, and compressive on the concave surfaces below the neutral plane).[168] Strain also appears during deformation associated with thermal expansion and contraction.[51] Tensile strains can produce cracks in all layers of the device and concomitant delamination if one layer deforms more than another in response to the same stress. Cracks in either the anode or cathode increase the series resistance of the device, and lower the fill factor and short-circuit current; thin areas in the active layers, or any scenario in which the electrodes are brought closer together, decrease the parallel (i.e., shunt) resistance, and also lower the fill factor and tend to decrease the open-circuit voltage. Catastrophic debonding of the electrodes produce open circuits, while cracks in the active layer that permit the electrodes to make physical contact produce short circuits,[28, 30] for which the *J–V* plots resemble resistors in parallel with photovoltaic cells (as in **Figures 12b** and **12c**).[31] In another example, Nickel et al. attributed cracking of a composite PEDOT:PSS/silver nanowire electrode as the source of degradation of a device based on a PTB7:$PC_{71}BM$ active layer while strained, but the device lost only 10% of its initial performance even at 14% strain.[169] It thus possible in principle for a solar cell to retain function even if the electrodes and the active materials are cracked all the way through, as long as the pathways leading to the electrodes are not interrupted. Compressive strain can also crack layers, especially of brittle materials, such as films of small molecule semiconductors (as observed by Tahk et al., **Figure 13a**).[32] Wrinkling of the surface (**Figure 13b**) can also occur under compressive strain if there is a mismatch in elasticity between the device layers and the substrate, or if the layers are poorly adhered.[51]

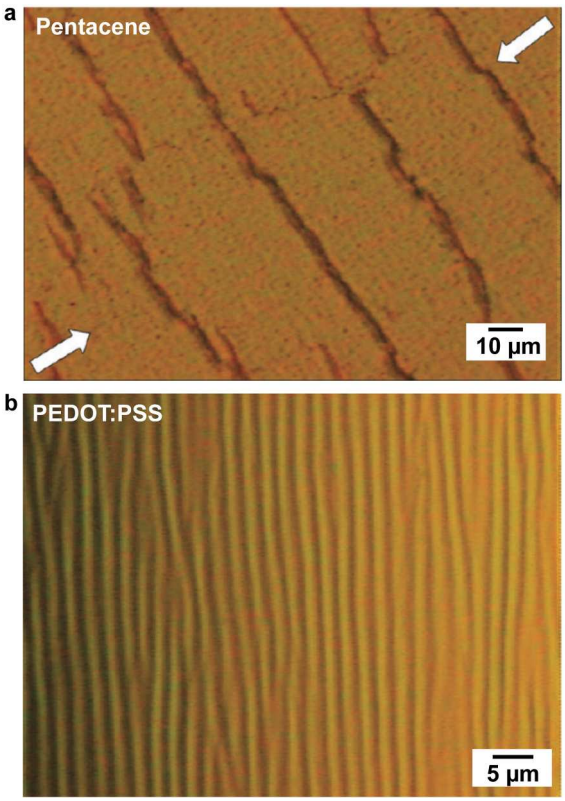

Figure 13. Images of cracks and buckles that appear in organic thin-film devices. (a) A cracked film of pentacene evaporated on a PDMS substrate and subjected to a 10% compressive strain. (b) A surface wrinkling pattern characteristic of the deformation that occurs in rigid films under compression due to direct application of mechanical force or because of thermal contraction. Reproduced with permission from ref.[32] Copyright 2009, American Chemical Society.

3.2.2. Strain applied normal to device plane

In contrast to the experiments described in this review so far, in which strain was applied in the plane of the device, the failure patterns of some types of devices may be predicted more realistically by experiments in which stress is applied perpendicular to the plane of the device. Stressing a multilayered device in this way can produce cohesive (within-layer) or adhesive (between-layer) failure. The Dauskardt laboratory published a series of studies that related the cohesive or adhesive fracture energy—G_c, the work needed to break or separate polymer films or interfaces—to various molecular parameters and processing conditions (**Figure 14**).[23, 50, 52, 68-70] The authors generally used a four-point bending test (**Figure 14a**) or double cantilever beam

apparatus to apply strain perpendicular to the plane of the device. The setup is intended to mimic modes of deformation that lead to separation within the device plane. Several important conclusions were drawn from this research that establish important design rules for improved reliability and yield of production of OPV devices.

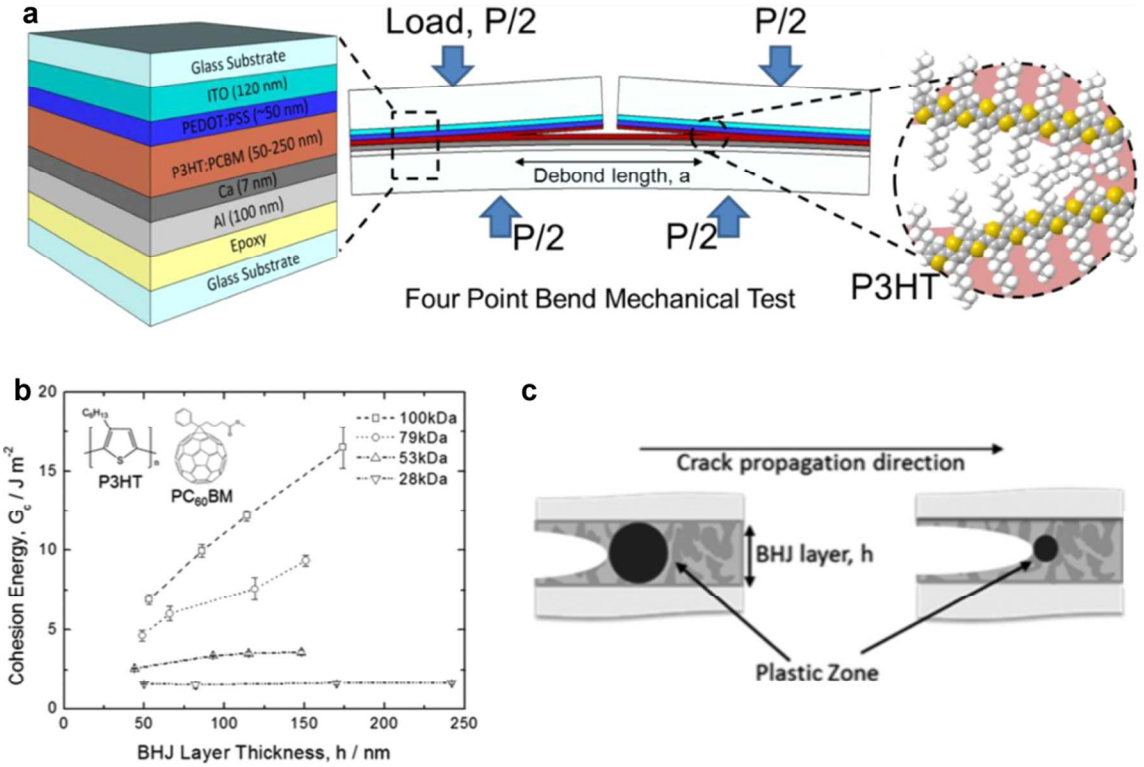

Figure 14. Schematic diagrams and data summarizing cohesive and delaminative fracture under different conditions. (a) Schematic diagram of the four bend mechanical test designed to measure the cohesive fracture energy of the P3HT:PCBM active layer in an organic solar cell as a function of molecular weight of the P3HT. (b) Cohesive energy vs. thickness of the BHJ layer with different molecular weights. Extremely high values of cohesion were obtained for thick films of high molecular weight. (c) Schematic illustration of the effect of the size of the plastic zone at the crack tip on the cohesion; brittle materials with small plastic zones exhibit less of a dependence on layer thickness, because the plastic zone is smaller than the distance between plates. Reproduced with permission from ref.[50] Copyright 2014, American Chemical Society.

The range of values of G_c for cohesion of the P3HT:fullerene bulk heterojunction were found to be 1–20 J m^{-2}, although the high end of this range was only measured for P3HT:ICBA[23] and in systems of thick P3HT:PCBM films in which the P3HT had high molecular weight.[50]

Typical values of 1–5 J m^{-2} are lower (more unfavorable) than those of other dielectric materials—e.g., crosslinked polymers and oxides—commonly used in microelectronics.[52] The cohesion was found to be strongly dependent on the composition of the bulk heterojunction. In particular, cohesion decreased with increasing PCBM concentration, from 0.5 J m^{-2} for pure PCBM to a maximum of 2.5 J m^{-2} for BHJs containing 75% P3HT.[52] The cohesive energy was not found to be affected by thickness, at least in the initial report, which the authors noted was different from the behavior of more-ductile polymers.[52] The cohesion, trajectory of the propagation of the crack, and the roughness after cohesive fracture depends on the mechanical properties of the material encountered by the crack during propagation. In examples of polymers exhibiting substantial plasticity (e.g., high-molecular-weight P3HT, **Figure 14b**), a plastic zone forms at the crack tip and expands until it is confined by either crystalline domains in the film or by the rigid top and bottom substrate (**Figure 14c**)—i.e., glass or epoxy in these experiments.[52] This plastic zone dissipates energy of the deformation, and decreases the cohesion measured in thin films of polymers with high ductility as thickness decreases, in which the volume of the plastic zone is confined by the hard substrate and backing.[50, 52] Dependence of cohesion on thickness is, however, present in high molecular weight P3HT,[50] which is consistent with a lowered degree of crystallinity and a larger plastic zone of the crack tip that is relatively unconstrained by rigid crystallites of samples with lower molecular weight. Formation of bimolecular crystals, in the case of PQT-12 and PBTTT and their mixtures with monofunctionalized PCBM, tends to produce bulk heterojunction films with relatively high cohesion ($G_c \sim 2–5$ J m^{-2}).[23] While this is an important observation that informs the selection of materials for mechanical robustness, bulk heterojunctions with bimolecular crystals at ratios of polymer:fullerene of 1:1 (i.e., below the concentration at which pure PCBM domains form) are

inefficient, and those with ratios of 1:4 fail cohesively more readily ($G_c \sim 1$ J m^{-2}) because of the fragility of the pure PCBM phase.[23]

In roll-to-roll processed flexible devices with the inverted architecture, adhesive failure was found to occur most commonly between the bulk heterojunction layers and PEDOT:PSS, with values of G_c between 0.1 to 1.6 J m^{-2}.[68] The adhesion decreased with increasing concentration of PCBM, which can be attributed to low interaction volume of fullerenes[100] and relatively weak van der Waals attraction to adjacent layers. We note that the order in which the layers are deposited has an effect on mechanical stability. For cells with the conventional geometry, in which the P3HT:PCBM is coated on top of the PEDOT:PSS, this interface survived, whereas the P3HT:PCBM failed cohesively.[52] The adhesion in the inverted geometry could be increased by increasing the time and temperature of annealing, or by replacing the PEDOT:PSS with another hole-transporting layer, such as vanadium oxide (V_2O_5). Use of V_2O_5, deposited from solution, produced an interface that was dramatically stronger (up to 150 J m^{-2}), but a device that was very inefficient.[68] Increased adhesion was attributed to a 10-nm-thick mixed layer between V_2O_5 and P3HT:PCBM. Depth profiling XPS determined that failure occurred between this mixed layer and the active layer. Reduced mixing and a weaker interface was found when solution processed V_2O_5 was replaced with vapor-deposited molybdenum oxide (MoO_3).[69] A mixed interfacial layer has also been invoked to explain the good adhesion between PEDOT:PSS and the active layer, if the PEDOT:PSS has been deposited first, and is possibly concomitant with the formation of P3HT$^+$:PSS$^-$ species where the polymer chains interact.[69] (The pure PEDOT:PSS phase itself is, however, subject to decohesion that accelerates in the presence of atmospheric moisture, attributed by DuPont et al. to hydrogen bonds of PSS$^-$ to water which disrupt the existing PSS$^-$---H$^+$---PSS$^-$ that give the polymer its cohesive strength.[70])

4. Possible routes of increasing the mechanical stability of organic solar cells

The experiments described in this review point to several routes that can be explored toward the end goal of increasing the mechanical robustness of organic solar cells. We identify several approaches that have been proposed explicitly or suggested by the results of experiments in the literature, and comment on the probability of success in a large-scale environment.

4.1. Buckled or wavy solar cells

The concepts introduced by Whitesides,[90] Rogers,[170] Wagner[171, 172] and others,[173] involving the production of thin-film devices whose active materials are buckled on pre-strained surfaces, and which accommodate strain by local bending and unbending of the buckles, has been exploited by Lipomi et al.[145] and then later by Kaltenbrunner et al.[3] to form unencapsulated stretchable organic solar cells. (Buckles and deep folds were later used as structures to increase light trapping by Loo and coworkers.[174]) This concept would be difficult to apply in a roll-to-roll scheme, because of the requirement that the substrate be under tension and the low probability that a multilayered device could be buckled by compressive strain without introducing substantial interfacial stress. The authors' experience suggests that under compressive strain, metallic electrodes, or solution processed oxides to modify the work function of one or more of the electrodes, would almost certainly crack and have a deleterious effect on the photovoltaic output of the devices. Furthermore, surface wrinkling requires a substantial mismatch in moduli between the substrate (~1 MPa for PDMS) and the thin films (≥10 MPa). The use of such deformable substrates in roll-to-roll coating apparatuses may not be straightforward.

4.2. Use of highly compliant conjugated polymers

A promising strategy to increase the mechanical robustness of OPV devices is to increase the elasticity, plasticity, or both, of the conjugated polymer. The highly compliant nature of P3HpT, a material with well ordered crystalline aggregates, is attributed to the amorphous domains whose glass transition is below room temperature, and suggests one possible way to achieve the "best of both worlds" of electronic and mechanical properties.[27] Another strategy is to take a material with a low bandgap and high mobility (such as a DPP-based material depicted in **Figure 1**) and introduce unlike conjugated monomers at random into the backbone, to decrease the degree of crystallinity (which would be effective so long as the material maintained high charge-carrier mobility in the absence of high crystallinity).[29] In general, factors that increase the compliance and ductility (independent of their effects on charge transport) are long alkyl side chains,[57] high molecular weight (at least in P3HT),[50] substitution of fused rings in the polymer backbone to isolated rings,[31] and structural randomness to reduce the degree of crystallinity.[29] All things being equal, highly cohesive and non-brittle conjugated polymers will perform better than brittle ones. The extent to which one component of the active material influences the failure behavior of the entire device, however, is an open question, and requires more testing. It also requires knowledge of the effects of other materials not only in the device stack, but within the active layer itself.

4.3. Substitution of PCBM

The ubiquitous acceptor PCBM has many deleterious effects on the mechanical stability of OPV devices. Pure PCBM phases have low cohesive energy,[52] high tensile moduli,[125] low crack-onset strains,[125] and weak interfaces with other layers in the device.[68] They can also

substantially stiffen active materials that have low moduli by themselves (e.g., P3HpT).[27] Decreasing the purity of the fullerene might suppress crystallization and therefore reduce the modulus, but this is not a guaranteed strategy.[125] Another potential route would be to find a different acceptor,[136] but our (very) preliminary observations on the mechanical properties of solution-processed small molecule films suggest that they are brittle. Polymer:polymer heterojunctions[59, 175] might represent a way forward, and indeed all-polymer solar cells have achieved high efficiencies in trials by several groups.[176, 177] The mechanical properties of electron-acceptor polymers are relatively unexplored, but we suspect that the design rules for robust donors would be easily translated to acceptors.

4.4. Plasticizers

The use of plasticizers represents an approach that is familiar to the engineering plastics community. For example, small molecules that increase the free volume in a polymer sample also tend to reduce its T_g and modulus, and increase its ductility. As discussed in Section 2.2.4, our group has found that compounds that are added to bulk heterojunction blends to increase efficiency (for example DIO or PDMS)[28] and to PEDOT:PSS to improve conductivity and wettability (DMSO or Zonyl),[71] can also have plasticizing effects on thin films. Since only a few plasticizers have been thoroughly tested in a laboratory setting, their success leads us to believe other combinations of additives could play a key role in improving mechanical stability. The effect of these plasticizers on the failure mechanisms of whole devices, however, is an open question; plasticizers may segregate to the surface and change the interfacial adhesive properties.[68] Another question is mechanistic: do these additives increase the compliance and

ductility simply by increasing the free volume (if they remain in the film) or by altering the morphology or extent of mixing, or some combination thereof?

4.5. Importance of adhesion

Strong interlayer adhesion is an important design characteristic, irrespective of the mechanical properties of the isolated materials. Interlayer adhesion[68] is generally increased if at least one of the interacting partners has a high surface energy, which is typically produced by a high dipolar contribution to the van der Waals coefficient of the material. Specific interactions, such as hydrogen bonding surfaces could also increase the adhesive fracture energy of the interfaces. Adhesion promoters would be beneficial, provided they do not have deleterious effects on charge transport in the device stack. In some cases, materials behave as serendipitous "prime coats," which is the case for PEDOT:PSS,[30] which improves the adhesion of bulk heterojunction films to hydrophobic substrates.[142]

4.6. Toward standardization of mechanical testing

As of yet, there is no standardized procedure for characterization of the mechanical stability of organic solar cells. Any international standards must begin with a full description of the dimensions and composition of all layers in the device, and the way in which it was processed. In particular, the order in which layers are processed will influence which materials or interfaces fail. The temperature and relative humidity must be reported, as the mechanical properties of the materials can be highly sensitive to these parameters. Devices intended for outdoor use must be tested for the effects of thermal cycling, and the effects of thermal expansion and contraction should be isolated from those that occur because of thermal cycling

independent of the concomitant mechanical deformation. Bending and tensile tests should be performed in a way that most realistically mimics the deformation expected in the environment. Simply reporting bending radius is insufficient for tests of flexibility; the depth of the active materials within the device stack must be specified, and their proximity to the mechanically neutral plane should be stated so that it is possible to calculate—in most cases by finite-element modeling—the strain on the active materials. Stresses that will produce cracks within or between layers will be highly dependent on the mechanical properties of the substrates and encapsulants. For devices on flexible substrates, torsion should also be tested, and the angle of torsion (e.g., 180° vs 360°) and number of cycles should be reported. Diligence in reporting these parameters will allow for a more thorough understanding of failure mechanisms and streamline the process for developing robust organic electronic devices.

5. Outlook and future work

The majority of all work on the stability of organic electronic devices in general—and organic solar cells in particular—has focused on photochemical, thermal, oxidative, morphological, and other thermodynamic modes of degradation.[20, 21] The exclusion of mechanical modes of degradation is somewhat surprising, because both the production and use of thin-film flexible solar modules requires—often substantial—bending, shear, and tensile deformations and thus requires resistance or at least a predictable response to mechanical strain. This review described the literature on the mechanical response of organic semiconductors and whole devices with the aim of identifying design principles for robust materials and devices to determine avenues of future research on the topic. We find several areas in which very little work has been done. For example, while the mechanical properties of polymers is a mature field,

and many of the principles can be applied directly to the properties of semiconducting polymers, the mechanical properties of films of small-molecule semiconductors and their effects on the yield of devices in roll-to-roll production are unexplored.

Much of the work has focused on the mechanical properties of single materials or interfaces. Only one study to our knowledge used a module fabricated in an industrially relevant manner.[68] The study of whole modules will require a close connection between experiments and computational modeling to determine which materials will absorb strain at different depths within the device stack. It might turn out, for example, that the barrier foils, which are often multilayered laminate structures of polymers and ceramic films, will crack first, and thus mechanical deformation may lead to failure by photochemical damage. As the field has not yet "settled" on the ideal barrier technology, attention toward the mechanical properties of barrier materials should be increased.

In the past, thermal stability has implied accelerated degradation by chemical processes, or by phase segregation within the bulk heterojunction. The suspected mechanism by which phase separation degrades the performance of solar cells is that the domains grow to critical dimensions that are larger than the diffusion lengths of excitons. Phase segregation is not, however, the only potential pathway of degradation initiated by heat. Differential thermal expansion and contraction of the different layers in an outdoor environment will inevitably produce large-scale buckling of support structures in pilot organic photovoltaic installations, just as smaller scale deformations will tend to place shear stress on the layers and could be especially problematic for the interfaces, which are often weak.

While the topics discussed in this review suggest that all deformation leads to fracture and therefore is deleterious to the long-term stability of devices, it is conceivable that strain in the

pre-fracture regime may produce changes that are either non-degrading or perhaps even beneficial to the photovoltaic output of devices. Very little is known about the effects of strain on device performance in the pre-fracture regime, but some ideas can be put forth. For example, strain has at least three effects on the morphology of P3HT:PCBM blends (as illustrated in **Figure 12**): (1) alignment of polymer chains along the axis of strain, (2) increase in the percentage of crystalline aggregates and order within the aggregated phase, and (3) evolution in texture from one in which the axis of π-stacking is parallel to the substrate (edge-on), to one in which the π-stacking axis is perpendicular to the substrate (face-on). While it is difficult to predict the effect of (1) on the photovoltaic properties, since the direction of charge-transport is orthogonal to the stretch-aligned chains, the effects of (2), and especially (3), would seem to be beneficial in a device whose charge carriers move vertically through the stack.

One intriguing aspect of research on the mechanical stability of organic solar cells is its interdisciplinarity. It requires teams whose members have expertise in organic chemistry, microstructural determination, polymeric science and engineering, device physics, manufacturing engineering, and solid mechanics. It is our hope that this review served to stimulate interest in the field in an effort to produce low-cost renewable power sources that are both highly efficient and also mechanically stable.

Acknowledgements

This work was supported by the Air Force Office of Scientific Research (AFOSR) Young Investigator Program, Grant FA9550-13-1-0156 and laboratory startup funds from the University of California, San Diego. S.S. acknowledges a fellowship from the National Science Foundation Graduate Research Fellowship Program under Grant DGE-1144086. A.V.Z. acknowledges a

fellowship from SoCal Clean Energy Technology Acceleration Program from the von Liebig Center at UCSD sponsored by the U.S. Department of Energy. The authors acknowledge helpful discussions with Prof. Frederik C. Krebs.

References

1. L. T. Dou, J. B. You, Z. R. Hong, Z. Xu, G. Li, R. A. Street and Y. Yang, *Adv. Mater.*, 2013, **25**, 6642-6671.

2. C. H. Peters, I. T. Sachs-Quintana, J. P. Kastrop, S. Beaupre, M. Leclerc and M. D. McGehee, *Adv. Energy Mater.*, 2011, **1**, 491-494.

3. M. Kaltenbrunner, M. S. White, E. D. Glowacki, T. Sekitani, T. Someya, N. S. Sariciftci and S. Bauer, *Nat. Comm.*, 2012, **3**, 770.

4. N. Espinosa, M. Hosel, D. Angmo and F. C. Krebs, *Energ. Environ. Sci.*, 2012, **5**, 5117-5132.

5. T. R. Cook, D. K. Dogutan, S. Y. Reece, Y. Surendranath, T. S. Teets and D. G. Nocera, *Chem. Rev.*, 2010, **110**, 6474-6502.

6. Y. Galagan, E. W. C. Coenen, B. Zimmermann, L. H. Slooff, W. J. H. Verhees, S. C. Veenstra, J. M. Kroon, M. Jorgensen, F. C. Krebs and R. Andriessen, *Adv. Energy Mater.*, 2014, **4**, 1300498.

7. F. C. Krebs, N. Espinosa, M. Hosel, R. R. Sondergaard and M. Jorgensen, *Adv. Mater.*, 2014, **26**, 29-39.

8. D. J. Burke and D. J. Lipomi, *Energ. Environ. Sci.*, 2013, **6**, 2053-2066.

9. T. P. Osedach, T. L. Andrew and V. Bulovic, *Energ. Environ. Sci.*, 2013, **6**, 711-718.

10. F. C. Krebs, M. Jorgensen, K. Norrman, O. Hagemann, J. Alstrup, T. D. Nielsen, J. Fyenbo, K. Larsen and J. Kristensen, *Sol. Energy Mater. Sol. Cells*, 2009, **93**, 422-441.

11. F. C. Krebs, *Sol. Energy Mater. Sol. Cells*, 2008, **92**, 715-726.

12. K.-S. Chen, H. L. Yip, C. W. Schlenker, D. S. Ginger and A. K. Y. Jen, *Org. Electron.*, 2012, **13**, 2870-2878.

13. I. Burgues-Ceballos, F. Machui, J. Min, T. Ameri, M. M. Voigt, Y. N. Luponosov, S. A. Ponomarenko, P. D. Lacharmoise, M. Campoy-Quiles and C. J. Brabec, *Adv. Funct. Mater.*, 2014, **24**, 1449-1457.

14. J. E. Carle, M. Helgesen, M. V. Madsen, E. Bundgaard and F. C. Krebs, *J. Mater. Chem. C*, 2014, **2**, 1290-1297.

15. R. Po, A. Bernardi, A. Calabrese, C. Carbonera, G. Corso and A. Pellegrino, *Energy Environ. Sci.*, 2014, **7**, 925-943.

16. J. L. Bredas, J. E. Norton, J. Cornil and V. Coropceanu, *Acc. Chem. Res.*, 2009, **42**, 1691-1169.

17. A. J. Heeger, *Adv. Mater.*, 2014, **26**, 10-28.

18. A. Salleo, R. J. Kline, D. M. DeLongchamp and M. L. Chabinyc, *Adv. Mater.*, 2010, **22**, 3812-3838.

19. M. A. Brady, G. M. Su and M. L. Chabinyc, *Soft Matter*, 2011, **7**, 11065-11077.

20. M. Jorgensen, K. Norrman and F. C. Krebs, *Sol. Energy Mater. Sol. Cells*, 2008, **92**, 686-714.

21. M. Jorgensen, K. Norrman, S. A. Gevorgyan, T. Tromholt, B. Andreasen and F. C. Krebs, *Adv. Mater.*, 2011, **24**, 580-612.

22. D. J. Lipomi and Z. N. Bao, *Energ. Environ. Sci.*, 2011, **4**, 3314-3328.

23. C. Bruner, N. C. Miller, M. D. McGehee and R. H. Dauskardt, *Adv. Funct. Mater.*, 2013, **23**, 2863-2871.

24. O. Awartani, B. Lemanski, H. W. Ro, L. J. Richter, D. M. DeLongchamp and B. T. O'Connor, *Adv. Energy Mater.*, 2013, **3**, 399-406.

25. M. Hosel, R. Sondergaard, M. Jorgensen and F. C. Krebs, *Adv. Energy Mater.*, 2014, **4**, 1301625.

26. F. C. Krebs, T. D. Nielsen, J. Fyenbo, M. Wadstrom and M. S. Pedersen, *Energ. Environ. Sci.*, 2010, **3**, 512-525.

27. S. Savagatrup, A. D. Printz, D. Rodriquez and D. J. Lipomi, *Macromolecules*, 2014, **47**, 1981-1992.

28. S. Savagatrup, A. S. Makaram, D. J. Burke and D. J. Lipomi, *Adv. Funct. Mater.*, 2014, **24**, 1169-1181.

29. A. D. Printz, S. Savagatrup, D. J. Burke, T. Purdy and D. J. Lipomi, *RSC Adv.*, 2014, **4**, 13635-13643.

30. T. F. O'Connor, A. V. Zaretski, B. A. Shiravi, S. Savagatrup, A. D. Printz, M. I. Diaz and D. J. Lipomi, *Energy Environ. Sci.*, 2014, **7**, 370-378.

31. D. J. Lipomi, H. Chong, M. Vosgueritchian, J. G. Mei and Z. N. Bao, *Sol. Energy Mater. Sol. Cells*, 2012, **107**, 355-365.

32. D. Tahk, H. H. Lee and D. Y. Khang, *Macromolecules*, 2009, **42**, 7079-7083.

33. B. O'Connor, E. P. Chan, C. Chan, B. R. Conrad, L. J. Richter, R. J. Kline, M. Heeney, I. McCulloch, C. L. Soles and D. M. DeLongchamp, *ACS Nano*, 2010, **4**, 7538-7544.

34. C. Muller, S. Goffri, D. W. Breiby, J. W. Andreasen, H. D. Chanzy, R. A. J. Janssen, M. M. Nielsen, C. P. Radano, H. Sirringhaus, P. Smith and N. Stingelin-Stutzmann, *Adv. Funct. Mater.*, 2007, **17**, 2674-2679.

35. J. J. Liang, L. Li, X. F. Niu, Z. B. Yu and Q. B. Pei, *Nat. Photonics*, 2013, **7**, 817-824.

36. Z. B. Yu, Q. W. Zhang, L. Li, Q. Chen, X. F. Niu, J. Liu and Q. B. Pei, *Adv. Mater.*, 2011, **23**, 664-668.

37. B. Hu, *Workshop on Key Scientific and Technological Issues for Development of Next-Generation Organic Solar Cells*, Arlington, VA, 2012.

38. F. C. Krebs, M. Biancardo, B. Winther-Jensen, H. Spanggard and J. Alstrup, *Sol. Energy Mater. Sol. Cells*, 2006, **90**, 1058-1067.

39. A. Anctil, C. W. Babbitt, R. P. Raffaelle and B. J. Landi, *Prog. Photovolt: Res. Appl.*, 2012, **DOI: 10.1002/pip**.

40. N. S. Lewis and D. G. Nocera, *Proc. Natl. Acad. Sci. USA*, 2007, **104**, 20142-20142.

41. J. Y. Lee, S. T. Connor, Y. Cui and P. Peumans, *Nano Lett.*, 2010, **10**, 1276.

42. G. Li, R. Zhu and Y. Yang, *Nat. Photonics*, 2012, **6**, 153-161.

43. C. M. Amb, M. R. Craig, U. Koldemir, J. Subbiah, K. R. Choudhyry, S. A. Gevorgyan, M. Jorgensen, F. C. Krebs, F. So and J. R. Reynolds, *ACS Appl. Mater. Interfaces*, 2012, **4**, 1847-1853.

44. V. Coropceanu, J. Cornil, D. A. da Silva, Y. Olivier, R. Silbey and J. L. Bredas, *Chem. Rev.*, 2007, **107**, 926-952.

45. S. Savagatrup, A. D. Printz, T. F. O'Connor, A. V. Zaretski and D. J. Lipomi, *Chem. Mater.*, 2014, **26**, 3028-3041.

46. S. Bauer, S. Bauer-Gogonea, I. Graz, M. Kaltenbrunner, C. Keplinger and R. Schwodiauer, *Adv. Mater.*, 2014, **26**, 149-162.

47. M. Kaltenbrunner, T. Sekitani, J. Reeder, T. Yokota, K. Kuribara, T. Tokuhara, M. Drack, R. Schwodiauer, I. Graz, S. Bauer-Gogonea, S. Bauer and T. Someya, *Nature*, 2013, **499**, 458-463.

48. D. Ghezzi, M. R. Antognazza, R. Maccarone, S. Bellani, E. Lanzarini, N. Martino, M. Mete, G. Pertile, S. Bisti, G. Lanzani and F. Benfanati, *Nat. Photonics*, 2013, **7**, 400-406.

49. M. Manceau, E. Bundgaard, J. E. Carle, O. Hagemann, M. Helgesen, R. Sondergaard, M. Jorgensen and F. C. Krebs, *J. Mater. Chem.*, 2011, **21**, 4132-4141.

50. C. Bruner and R. H. Dauskardt, *Macromolecules*, 2014, **47**, 1117-1121.

51. V. Brand, K. Levi, M. D. McGehee and R. H. Dauskardt, *Sol. Energy Mater. Sol. Cells*, 2012, **103**, 80-85.

52. V. Brand, C. Bruner and R. H. Dauskardt, *Sol. Energy Mater. Sol. Cells*, 2012, **99**, 182-189.

53. Y. Cao, P. A. Smith and A. J. Heeger, *Synthetic Met.*, 1991, **41-43**, 181-184.

54. Y. Cao, P. Smith and A. J. Heeger, *Polymer*, 1991, **32**, 1210-1218.

55. S. Tokito, P. Smith and A. J. Heeger, *Synthetic Met.*, 1990, **36**, 183-194.

56. A. R. Postema, K. Liou, F. Wudl and P. Smith, *Macromolecules*, 1990, **23**, 1842-1845.

57. J. Moulton and P. Smith, *Polymer*, 1992, **33**, 2340-2347.

58. G. Yu, J. Gao, J. C. Hummelen, F. Wudl and A. J. Heeger, *Science*, 1995, **270**, 1789-1791.

59. J. J. M. Halls, C. A. Walsh, N. C. Greenham, E. A. Marseglia, R. H. Friend, S. C. Moratti and A. B. Holmes, *Nature*, 1995, **376**, 498-500.

60. J. H. Burroughes, D. D. C. Bradley, A. R. Brown, R. N. Marks, K. Mackay, R. H. Friend, P. L. Burns and A. B. Holmes, *Nature*, 1990, **347**, 539-541.

61. A. Tsumura, H. Koezuka and T. Ando, *Appl. Phys. Lett.*, 1986, **49**, 1210-1212.

62. Z. N. Bao, A. Dodabalapur and A. J. Lovinger, *Appl. Phys. Lett.*, 1996, **69**, 4108-4110.

63. A. Facchetti, *Chem. Mater.*, 2011, **23**, 733-758.

64. J. G. Mei and Z. N. Bao, *Chem. Mater.*, 2014, **26**, 604-615.

65. H. Bronstein, Z. Y. Chen, R. S. Ashraf, W. M. Zhang, J. P. Du, J. R. Durrant, P. S. Tuladhar, K. Song, S. E. Watkins, Y. Geerts, M. M. Wienk, R. A. J. Janssen, T. Anthopoulos, H. Sirringhaus, M. Heeney and I. McCulloch, *J. Am. Chem. Soc*, 2011, **133**, 3272-3275.

66. I. McCulloch, M. Heeney, C. Bailey, K. Genevicius, I. MacDonald, M. Shkunov, D. Sparrowe, S. Tierney, R. Wagner, W. M. Zhang, M. L. Chabinyc, R. J. Kline, M. D. McGehee and M. F. Toney, *Nat. Mater.*, 2006, **5**, 328-333.

67. A. J. Heeger, *Chem. Soc. Rev.*, 2010, **39**, 2354-2371.

68. S. R. Dupont, M. Oliver, F. C. Krebs and R. H. Dauskardt, *Sol. Energy Mater. Sol. Cells*, 2012, **97**, 171-175.

69. S. R. Dupont, E. Voroshazi, P. Heremans and R. H. Dauskardt, *Org. Electron.*, 2013, **14**, 1262-1270.

70. S. R. Dupont, F. Novoa, E. Voroshazi and R. H. Dauskardt, *Adv. Funct. Mater.*, 2013, **24**, 1325-1332.

71. S. Savagatrup, E. Chan, S. Renteria-Garcia, A. D. Printz, A. V. Zaretski, T. F. O'Connor, D. Rodriquez, E. Valle and D. J. Lipomi, *Adv. Funct. Mater.,* 2014, accepted.

72. A. J. Heeger, *Angew. Chem., Int. Ed.*, 2001, **40**, 2591-2611.

73. S. M. Aharoni, *Polymer*, 1981, **22**, 418-419.

74. R. D. McCullough, *Adv. Mater.*, 1998, **10**, 93-116.

75. F. P. V. Koch, M. Heeney and P. Smith, *J. Am. Chem. Soc*, 2013, **135**, 13699-13709.

76. M. Brinkmann, *Polym. Phys.*, 2011, **49**, 1218-1233.

77. J. Rivnay, M. F. Toney, Y. Zheng, I. V. Kauver, Z. H. Chen, V. Wagner, A. Facchetti and A. Salleo, *Adv. Mater.*, 2010, **22**, 4359-4363.

78. B. O'Connor, R. J. Kline, B. R. Conrad, L. J. Richter, D. Gundlach, M. F. Toney and D. M. DeLongchamp, *Adv. Funct. Mater.*, 2011, **21**, 3697-3705.

79. D. Gargi, R. J. Kline, D. M. DeLongchamp, D. A. Fischer, M. F. Toney and B. T. O'Connor, *J. Phys. Chem. C*, 2013, **117**, 17421-17428.

80. O. Awartani, M. W. Kudenov and B. T. O'Connor, *Appl. Phys. Lett.*, 2014, **104**, 093306.

81. F. E. Arnold and Vandeuse.Rl, *Macromolecules*, 1969, **2**, 497-&.

82. M. R. Vanlandingham, J. S. Villarrubia, W. F. Guthrie and G. F. Meyers, *Macromol. Symp.*, 2001, **167**, 15-43.

83. P. G. Karagiannidis, S. Kassavetis, C. Pitsalidis and S. Logothetidis, *Thin Solid Films*, 2011, **519**, 4105-4109.

84. C. Koidis, S. Logothetidis, S. Kassavetis, P. G. Kapnopoulos, P. G. Karagiannidis, D. Georgiou and A. Laskarakis, *Sol. Energy Mater. Sol. Cells*, 2013, **112**, 36-46.

85. J. Y. Chung, A. J. Nolte and C. M. Stafford, *Adv. Mater.*, 2011, **23**, 349-368.

86. C. M. Stafford, C. Harrison, K. L. Beers, A. Karim, E. J. Amis, M. R. Vanlandingham, H. C. Kim, W. Volksen, R. D. Miller and E. E. Simonyi, *Nat. Mater.*, 2004, **3**, 545-550.

87. C. M. Stafford, B. D. Vogt, C. Harrison, D. Julthongpiput and R. Huang, *Macromolecules*, 2006, **39**, 5095-5099.

88. D. Y. Khang, J. A. Rogers and H. H. Lee, *Adv. Funct. Mater.*, 2009, **19**, 1526-1536.

89. D. Y. Khang, J. L. Xiao, C. Kocabas, S. MacLaren, T. Banks, H. Q. Jiang, Y. Y. G. Huang and J. A. Rogers, *Nano Lett.*, 2008, **8**, 124-130.

90. N. Bowden, S. Brittain, A. G. Evans, J. W. Hutchinson and G. M. Whitesides, *Nature*, 1998, **393**, 146-149.

91. N. Bowden, W. T. S. Huck, K. E. Paul and G. M. Whitesides, *Appl. Phys. Lett.*, 1999, **75**, 2557-2559.

92. J.-B. Lee, S.-S. Yoon and D. Y. Khang, *RSC Adv.*, 2013, **3**, 17364-17372.

93. J. Y. Kim and C. D. Frisbie, *J. Phys. Chem. C*, 2008, **112**, 17726-17736.

94. J. Zhao, A. Swinnen, G. V. Assche, J. Manca, D. Vanderzande and B. V. Mele, *J. Phys. Chem. B*, 2009, **113**, 1587-1591.

95. S. A. Chen and J. M. Ni, *Macromolecules*, 1992, **25**, 6081-6089.

96. H. K. Reimschuessel, *J. Polym. Sci. A: Polym. Chem.*, 1979, **17**, 2447-2457.

97. M. Koppe, M. Scharber, C. J. Brabec, W. Duffy, M. Heeney and I. McCulloch, *Adv. Funct. Mater.*, 2007, **17**, 1371-1376.

98. A. Buono, N. H. Son, G. Raos, L. Gila, A. Cominetti, M. Catellani and S. V. Meille, *Macromolecules*, 2010, **43**, 6772-6781.

99. J. G. Liu, Y. Sun, X. Gao, R. Xing, L. D. Zheng, S. P. Wu, Y. H. Geng and Y. C. Han, *Langmuir*, 2011, **27**, 4212-4219.

100. J. N. Israelachvili, *Intermolecular and Surface Forces*, Elsevier, Waltham, MA, 2011.

101. H. L. Zhong, Z. Li, F. Deledalle, E. Collado Fregoso, M. Shahid, Z. P. Fei, C. B. Nielsen, N. Yaacobi-Gross, S. Rossbauer, T. D. Anthopoulos, J. R. Durrant and M. Heeney, *J. Am. Chem. Soc*, 2013, **135**, 2040.

102. D. J. Lipomi, R. C. Chiechi, W. F. Reus and G. M. Whitesides, *Adv. Funct. Mater.*, 2008, **18**, 3469-3477.

103. D. J. Lipomi, R. C. Chiechi, M. D. Dickey and G. M. Whitesides, *Nano Lett.*, 2008, **8**, 2100-2105.

104. F. S. Kim, G. Q. Ren and S. A. Jenekhe, *Chem. Mater.*, 2011, **23**, 682-732.

105. A. L. Briseno, S. C. B. Mannsfeld, P. J. Shamberger, F. S. Ohuchi, Z. N. Bao, S. A. Jenekhe and Y. N. Xia, *Chem. Mater.*, 2008, **20**, 4712-4719.

106. J. T. Seitz, *J. Appl. Polym. Sci.*, 1993, **49**, 1331-1351.

107. R. F. Fedors, *Polym. Eng. Sci.*, 1974, **14**, 147-154.

108. B. S. Hsiao, *Nanostructure development in semicrystalline polymers during deformation by synchrotron X-ray scattering and diffraction techniques*, Taylor & Francis, 2005.

109. S. T. Salammal, E. Mikayelyan, S. Grigorian, U. Pietsch, N. Koenen, U. Scherf, N. Kayunkid and M. Brinkmann, *Macromolecules*, 2012, **45**, 5575-5585.

110. F. Padinger, R. S. Rittberger and N. S. Sariciftci, *Adv. Funct. Mater.*, 2003, **13**, 85-88.

111. S. E. Shaheen, C. J. Brabec, N. S. Sariciftci, F. Padinger, T. Fromherz and J. C. Hummelen, *Appl. Phys. Lett.*, 2001, **78**, 841-843.

112. V. Vijay, A. D. Rao and K. S. Narayan, *J. Appl. Phys.*, 2011, **109**, 084525.

113. J. Rivnay, S. C. B. Mannsfeld, C. E. Miller, A. Salleo and M. F. Toney, *Chem. Rev.*, 2012, **112**, 5488-5519.

114. J. Clark, C. Silva, R. H. Friend and F. C. Spano, *Phys. Rev. Lett.*, 2007, **98**, 206406.

115. R. J. Kline, M. D. McGehee, E. N. Kadnikova, J. S. Liu, J. M. J. Frechet and M. F. Toney, *Macromolecules*, 2005, **38**, 3312-3319.

116. A. J. Pearson, T. Wang, A. D. F. Dunbar, H. N. Yi, D. C. Watters, D. M. Coles, P. A. Staniec, A. Iraqi, R. A. L. Jones and D. G. Lidzey, *Adv. Funct. Mater.*, 2013, **24**, 659.

117. N. C. Miller, R. Gysel, Z. Beiley, C. E. Miller, M. F. Toney, M. Heeney, I. McCulloch and M. D. McGehee, *Nano Lett.*, 2009, **9**, 4153-4157.

118. N. C. Miller, E. K. Cho, R. Gysel, C. Risko, V. Coropceanu, C. E. Miller, S. Sweetnam, A. Sellinger, M. Heeney, I. McCulloch, J. L. Bredas, M. F. Toney and M. D. McGehee, *Adv. Energy Mater.*, 2012, **2**, 1208-1217.

119. J. Rivnay, R. Noriega, R. J. Kline, A. Salleo and M. F. Toney, *Phys. Rev. B*, 2011, **84**, 045203.

120. E. Verploegen, R. Mondal, C. J. Bettinger, S. Sok, M. F. Toney and Z. Bao, *Adv. Funct. Mater.*, 2010, **20**, 3519-3529.

121. J. D. Roehling, K. J. Batenburg, F. B. Swain, A. J. Moule and I. Arslan, *Adv. Funct. Mater.*, 2013, **23**, 2115-2122.

122. W. Ma, J. R. Tumbleston, M. Wang, E. Gann, F. Huang and H. Ade, *Adv. Energy Mater.*, 2013, **3**, 864-872.

123. N. D. Treat, A. Varotto, C. J. Takacs, N. Batara, M. Al-Hashimi, M. J. Heeney, A. J. Heeger, F. Wudl, C. J. Hawker and M. L. Chabinyc, *J. Am. Chem. Soc*, 2012, **134**, 15869-15879.

124. N. D. Treat, M. A. Brady, G. Smith, M. F. Toney, E. J. Kramer, C. J. Hawker and M. L. Chabinyc, *Adv. Energy Mater.*, 2011, **1**, 82-89.

125. S. Savagatrup, D. Rodriquez, A. D. Printz, A. Sieval, J. C. Hummelen and D. J. Lipomi, *Submitted*, 2014.

126. L. H. Nguyen, H. Hoppe, T. Erb, S. Gunes, G. Gobsch and N. S. Sariciftci, *Adv. Funct. Mater.*, 2007, **17**, 1071-1078.

127. H. Hoppe and N. S. Sariciftci, *Journal of Materials Chemistry*, 2006, **16**, 45-61.

128. H. Hoppe, M. Niggemann, C. Winder, J. Kraut, R. Hiesgen, A. Hinsch, D. Meissner and N. S. Sariciftci, *Adv. Funct. Mater.*, 2004, **14**, 1005-1011.

129. F. Liu, Y. Gu, X. B. Shen, S. Ferdous, H. W. Wang and T. P. Russell, *Prog. Polym. Sci.*, 2013, **38**, 1990-2052.

130. H. W. Ro, B. Akgun, B. T. O'Connor, M. Hammond, R. J. Kline, C. R. Snyder, S. K. Satija, A. L. Ayzner, M. F. Toney, C. L. Soles and D. M. DeLongchamp, *Macromolecules*, 2012, **45**, 6587-6599.

131. A. D. Printz, S. Savagatrup, D. Rodriquez, T. F. O'Connor and D. J. Lipomi, *Sol. Energy Mater. Sol. Cells*, 2014, in press.

132. H. Y. Li, B. C.-K. Tee, G. Giri, J. W. Chung, S. Y. Lee and Z. N. Bao, *Adv. Mater.*, 2012, **24**, 2588-2591.

133. T. Liu and A. Troisi, *Adv. Mater.*, 2013, **25**, 1038-1041.

134. A. Anctil, C. W. Babbitt, R. P. Raffaelle and B. J. Landi, *Environ. Sci. Technol.*, 2011, **45**, 2353-2359.

135. Y.-S. Zimmermann, A. Schaffer, C. Hugi, K. Fent, P. F.-X. Corvini and M. Lenz, *Environ. Int.*, 2012, **49**, 128-140.

136. P. Sonar, J. P. F. Lim and K. L. Chan, *Energ. Environ. Sci.*, 2011, **4**, 1558-1574.

137. J. Peet, A. J. Heeger and G. C. Bazan, *Acc. Chem. Res.*, 2009, **42**, 1700-1708.

138. J. Peet, J. Y. Kim, N. E. Coates, W. L. Ma, D. Moses, A. J. Heeger and G. C. Bazan, *Nat. Mater.*, 2007, **6**, 497-500.

139. K. R. Graham, J. G. Mei, R. Stalder, J. W. Shim, H. Cheun, F. Steffy, F. So, B. Kippelen and J. R. Reynolds, *ACS Appl. Mater. Interfaces*, 2011, **3**, 1210-1215.

140. M. Vosgueritchian, D. J. Lipomi and Z. N. Bao, *Adv. Funct. Mater.*, 2012, **22**, 421-428.

141. N. Kim, S. Kee, S. H. Lee, B. H. Lee, Y. H. Kahng, Y. R. Jo, B. J. Kim and K. Lee, *Adv. Mater.*, 2014, **26**, 2268-2272.

142. D. J. Lipomi, J. A. Lee, M. Vosgueritchian, B. C.-K. Tee, J. A. Bolander and Z. N. Bao, *Chem. Mater.*, 2012, **24**, 373-382.

143. X. Crispin, F. L. E. Jakobsson, A. Crispin, P. C. M. Grim, P. Andersson, A. Volodin, C. van Haesendonck, M. Van der Auweraer, W. R. Salaneck and M. Berggren, *Chem. Mater.*, 2006, **18**, 4354-4360.

144. D. S. Hecht, L. B. Hu and G. Irvin, *Adv. Mater.*, 2011, **23**, 1482-1513.

145. D. J. Lipomi, B. C.-K. Tee, M. Vosgueritchian and Z. N. Bao, *Adv. Mater.*, 2011, **23**, 1771-1775.

146. M. M. Voigt, R. C. I. Mackenzie, C. P. Yau, P. Atienzar, J. Dane, P. E. Keivanidis, D. D. C. Bradley and J. Nelson, *Sol. Energy Mater. Sol. Cells*, 2011, **95**, 731-734.

147. Y. H. Zhou, C. Fuentes-Hernandez, J. W. Shim, J. Meyer, A. J. Giordano, H. Li, P. Winget, T. Papadopoulos, H. Cheun, J. Kim, M. Fenoll, A. Dindar, W. Haske, E. Najafabadi, T. M. Khan, H. Sojoudi, S. Barlow, S. Graham, J. L. Bredas, S. R. Marder, A. Kahn and B. Kippelen, *Science*, 2012, **336**, 327-332.

148. L. Lindell, A. Burquel, F. L. E. Jakobsson, V. Lemaur, M. Berggren, R. Lazzaroni, J. Cornil, W. R. Salaneck and X. Crispin, *Chem. Mater.*, 2006, **18**, 4246-4252.

149. F. L. E. Jakobsson, X. Crispin, L. Lindell, A. Kanciurzewska, M. Fahlman, W. R. Salaneck and M. Berggren, *Chem. Phys. Lett.*, 2006, **433**, 110-114.

150. J. E. Coughlin, Z. B. Henson, G. C. Welch and G. C. Bazan, *Acc. Chem. Res.*, 2013, **47**, 257-270.

151. M. Shin, J. H. Song, G. H. Lim, B. Lim, J. J. Park and U. Jeong, *Adv. Mater.*, 2014, **26**, 3706-3711.

152. Z. B. Yu, X. F. Niu, Z. Liu and Q. B. Pei, *Adv. Mater.*, 2011, **23**, 3989-3994.

153. G. Giri, E. Verploegen, S. C. B. Mannsfeld, S. Atahan-Evrenk, D. H. Kim, S. Y. Lee, H. A. Becerril, A. Aspuru-Guzik, M. F. Toney and Z. Bao, *Nature*, 2011, **480**, 504-509.

154. Y. Diao, B. C.-K. Tee, G. Giri, J. Xu, D. H. Kim, H. A. Becerril, R. M. Stoltenberg, T. H. Lee, G. Xue, S. C. B. Mannsfeld and Z. N. Bao, *Nat. Mater.*, 2013, **12**, 665-671.

155. Z. L. Rang, A. Haraldsson, D. M. Kim, P. P. Ruden, R. J. Chesterfield and C. D. Frisbie, *Appl. Phys. Lett.*, 2001, **79**, 2731-2733.

156. C.-Y. Liu and A. J. Bard, *Nature*, 2002, **418**, 162-164.

157. H. R. Tseng, H. Phan, C. Luo, M. Wang, L. A. Perez, S. N. Patel, L. Ying, E. J. Kramer, T. Q. Nguyen, G. C. Bazan and A. J. Heeger, *Adv. Mater.*, 2014, **online**, 10.1002/adma.201305084.

158. H. C. Wu, S. J. Benight, A. Chortos, W. Y. Lee, J. G. Mei, J. W. F. To, C. Lu, M. Q. He, J. B.-H. Tok, W. C. Chen and Z. N. Bao, *Chem. Mater.*, 2014, **dx.doi.org/10.1021/cm502271j**.

159. D. Chirvase, J. Parisi, J. C. Hummelen and V. Dyakonov, *Nanotechnology*, 2004, **15**, 1317-1323.

160. G. Li, Y. Yao, H. C. Yang, V. Shrotriya, G. W. Yang and Y. Yang, *Adv. Funct. Mater.*, **17**, 1636-1644.

161. A. N. Sokolov, Y. Cao, O. B. Johnson and Z. N. Bao, *Adv. Funct. Mater.*, 2012, **22**, 175-183.

162. N. S. Lu, X. Wang, Z. G. Suo and J. Vlassak, *Appl. Phys. Lett.*, 2007, **91**, 221909.

163. A. Chortos, J. Lim, J. W. F. To, M. Vosgueritchian, T. J. Dusseault, T. H. Kim, S. W. Hwang and Z. N. Bao, *Adv. Mater.*, 2014, **26**, 4253-4259.

164. A. L. Shu, A. Dai, H. Wang, Y. L. Loo and A. Kahn, *Org. Electron.*, 2013, **14**, 149-155.

165. A. Dai, Y. H. Zhou, A. L. Shu, S. K. Mohapatra, H. Wang, C. Fuentes-Hernandez, Y. D. Zhang, S. Barlow, Y. L. Loo, S. R. Marder, B. Kippelen and A. Kahn, *Adv. Funct. Mater.*, 2013, **24**, 2197-2204.

166. G. Lubineau and M. N. Saleh, *Sol. Energy Mater. Sol. Cells*, 2014, **130**, 199-207.

167. S. K. Hau, H. L. Yip, J. Y. Zou and A. K. Y. Jen, *Org. Electron.*, 2009, **10**, 1401-1407.

168. D. H. Kim and J. A. Rogers, *Adv. Mater.*, 2008, **20**, 4887-4892.

169. F. Nickel, T. Haas, E. Wegner, D. Bahro, S. Salehin, O. Kraft, P. A. Gruber and A. Colsmann, *Sol. Energy Mater. Sol. Cells*, 2014, **130**, 317-321.

170. W. M. Choi, J. Z. Song, D. Y. Khang, H. Q. Jiang, Y. Y. Huang and J. A. Rogers, *Nano Lett.*, 2007, **7**, 1655-1663.

171. J. Jones, S. P. Lacour, S. Wagner and Z. G. Suo, *J. Vac. Sci. Technol., A*, 2004, **22**, 1723-1725.

172. S. P. Lacour, S. Wagner, Z. Y. Huang and Z. Suo, *Appl. Phys. Lett.*, 2003, **82**, 2404-2406.

173. H. S. Wu, S. Kustra, E. M. Gates and C. J. Bettinger, *Org. Electron.*, 2013, **14**, 1636-1642.

174. J. B. Kim, P. Kim, N. C. Pegard, S. J. Oh, C. R. Kagan, J. W. Fleischer, H. A. Stone and Y. L. Loo, *Nat. Photonics*, 2012, **6**, 327-332.

175. X. M. He, F. Gao, G. Tu, D. Hasko, S. Huttner, U. Steiner, N. C. Greenham, R. H. Friend and W. T. S. Huck, *Nano Lett.*, 2010, **10**, 1302-1307.

176. W. W. Li, W. S. C. Roelofs, M. Turbiez, M. M. Wienk and R. A. J. Janssen, *Adv. Mater.*, 2014, **26**, 3304-3309.

177. Y. Zhou, T. Kurosawa, W. Ma, Y. K. Guo, L. Fang, K. Vandewal, Y. Diao, C. G. Wang, Q. F. Yan, J. Reinspach, J. G. Mei, A. L. Appleton, G. I. Koleilat, Y. L. Gao, S. C. B.

Mannsfeld, A. Salleo, H. Ade, D. H. Zhao and Z. N. Bao, *Adv. Mater.*, 2014, **26**, 3767-3772.

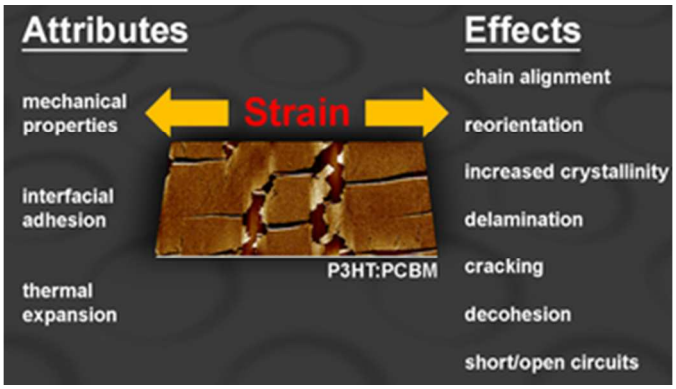

28x16mm (300 x 300 DPI)